DOKUZ EYLÜL UNIVERSITY
GRADUATE SCHOOL OF NATURAL AND APPLIED SCIENCES

EFFECT OF PLY ORIENTATION ON LOW VELOCITY IMPACT BEHAVIOUR OF WOVEN COMPOSITE STRUCTURES

by

Gökberk UÇAK

February, 2024

İZMİR

EFFECT OF PLY ORIENTATION ON LOW VELOCITY IMPACT BEHAVIOUR OF WOVEN COMPOSITE STRUCTURES

A Thesis Submitted to the
Graduate School of Natural and Applied Sciences of Dokuz Eylül University
In Partial Fulfillment of the Requirements for Master of Science in
Department of Mechanical Engineering, Mechanics Program

by

Gökberk UÇAK

February, 2024

İZMİR

THESIS EXAMINATION RESULT FORM

We have read the thesis entitled **"EFFECT OF PLY ORIENTATION ON LOW VELOCITY IMPACT BEHAVIOUR OF WOVEN COMPOSITE STRUCTURES"** completed by **GÖKBERK UÇAK** under supervision of **PROF.DR. RAMAZAN KARAKUZU** and we certify that in our opinion it is fully adequate, in scope and in quality, as a thesis for the degree of Master of Science.

Prof.Dr. Ramazan KARAKUZU

Supervisor

Prof. Dr. Yusuf ARMAN

Jury Member

Prof. Dr. Buket OKUTAN BABA

Jury Member

Prof. Dr. Okan FISTIKOĞLU

Director

Graduate School of Natural and Applied Sciences

ACKNOWLEDGMENT

Many people supported and helped me throughout my master education. First of all, I would like to thank my M.Sc supervisor, Prof. Dr. Ramazan KARAKUZU, leading me with his immense knowledge and experiences.

I would like to thanks to Dr. Mehmet KORKMAZ and Dr. Halis KANDAŞ for helping me producing and testing of my samples.

Also, I always felt my family members support during my education. I would like to thanks them.

Gökberk UÇAK

EFFECT OF PLY ORIENTATION ON LOW VELOCITY IMPACT BEHAVIOUR OF WOVEN COMPOSITE STRUCTURES

ABSTRACT

In designs where composite materials are used, in addition to resistance to static and dynamic loading, the reaction of the material to sudden impacts is also a critical parameter that should be taken into consideration. This resistance of the material is an important design criterion, especially in a wide perspective, from minor impact damages that occur during manufacturing to sudden and singular forces during the use of the final product.

Today, with the widespread use of composite materials in industrial use, especially in the aviation and automobile industries, this issue has become even more important. For this reason, studies have been carried out in this field according to the operating conditions of composite plates, plate thickness, fabric material, impact properties and impact energies.

Within the scope of this study, the reactions of E-glass reinforced resin composites, which are composite materials used in many areas in the industry, against impact tests and the relationship between the fiber orientations of the woven composite structures that make up this composite were examined.

The samples produced in this context, each made of seven layers of fabric, were manufactured in 4 different types; Type 1 ($[0/90/0/\overline{90}]_s$), type 2 ($[0/45/90/\overline{45}]_s$), type 3 ($[0/30/60/\overline{90}]_s$) and type 4 ([0/15/30/45/60/75/90]) These specimens produced by vacuum assisted resin infusion molding (VARIM) method. The impact energies to be applied on the composites were determined as 10J, 20J, 30J, 40J and 50J and tests were carried out at these impact energy values and the results were analyzed.

Keywords: Low velocity impact, fiber orientation, woven fabrics, penetration and perforation threshold

ÖRGÜ KOMPOZİT YAPILARIN DÜŞÜK HIZLI DARBE DAVRANIŞINA TABAKA ORYANTASYONUN ETKİSİ

ÖZ

Kompozit malzemelerin kullanıldığı tasarımlarda statik ve dinamik yüklemeye karşı dayanımının haricinde malzemenin ani darbelere karşı verdiği reaksiyon da göz önüne alınması gereken kritik bir parametredir. Özellikle imalat sırasında meydana gelen küçük darbe hasarlarından, son ürünün kullanımı sırasındaki ani ve tekil kuvvetlere kadar oldukça geniş bir perspektifte malzemenin göstermiş olduğu bu dayanım önemli bir tasarım kriteridir.

Günümüzde kompozit malzemelerin başta havacılık ve otomobil endüstrisinde olmak üzere endüstriyel kullanımının yaygınlaşmasıyla beraber bu konu daha da önem kazanmıştır. Bu sebeple bu alanda kompozit plakaların çalışma koşullarına, plaka kalınlıklarına, kumaş malzemesine, vurucu özelliklerine ve darbe enerjilerine göre çalışmalar yapılmıştır.

Bu çalışma kapsamında ise endüstride çok fazla alanda kullanılmakta olan kompozit malzemelerden örgülü E-glass ve reçine kompozitlerin darbe testlerine karşı verdikleri reaksiyonlar ile bu kompoziti oluşturan örgülü kompozit yapıların serim oryantasyonları ile arasındaki ilişki incelenmiştir.

Bu kapsamda yedişer kat kumaştan üretilmiş olan numuneler 4 farklı tipte imal edilmiştir. Tip 1 ($[0/90/0/\overline{90}]_s$), tip 2 ($[0/45/90/\overline{45}]_s$), tip 3 ($[0/30/60/\overline{90}]_s$) ve tip 4 ([0/15/30/45/60/75/90]) olarak bu numuneler vakum yardımıyla infüzyon metoduyla üretilmiştir. Kompozitler üzerinde uygulanacak darbe enerjileri 10J, 20J, 30J, 40J ve 50J olarak belirlenmiş ve bu darbe enerjisi değerlerinde testler uygulanmış ve sonuçlar analiz edilmiştir.

Anahtar kelimeler: Düşük hızlı darbe, fiber oryantasyonları, örgülü kumaş, saplanma ve delinme eşiği

CONTENTS

Page

THESIS EXAMINATION RESULT FORM ii
ACKNOWLEDGMENT iii
ABSTRACT iv
ÖZ v
CONTENTS vi
LIST OF FIGURES viii
LIST OF TABLES xi

CHAPTER ONE - INTRODUCTION 1

1.1 Introduction 1
1.2 Purpose & Scope 1

CHAPTER TWO - PREVIOUS STUDIES 3

CHAPTER THREE - METHODOLOGY AND ANALYSIS OF DATA 6

3.1 Contact Law 6
3.1.1 Hertz Contact Law 6
3.1.2 Contact Law for Laminates 7
3.2 Failure Modes 10
3.2.1 Delaminations 10
3.2.2 Matrix Cracks 11
3.2.3 Fiber Fractures 12
3.3 Impact Test Methods 12
3.3.1 Low Velocity Impact Test Methods 12
3.3.2 High Velocity Impact Test Methods 14
3.3.3 Ballistic Impact Test Methods 14
3.4 Responses of Composites in Impact Tests 15
3.4.1 Contact Force-Displacements Curves 15
3.4.2 Contact Force-Time Curves 18
3.4.3 Displacements-Time Curves 19

3.4.4 Velocity-Time Curves 20
3.4.5 Absorbed Energy-Time Curves 21

CHAPTER FOUR - PRE-EXPERİMENTAL PREPARATİONS 25

4.1 Sample Production 25
4.1.1 Fabric Preparation 25
4.1.2 Consumables 26
4.1.3 Fabrication 27
4.2 Test Device 31
4.3 Detection of the Impact energy to be Applied 34

CHAPTER FIVE RESULTS 36

5.1 Results 36
5.2 Conclusions 51

REFERENCES 53

LIST OF FIGURES

Page

Figure 3.1 Pressure on Contact Area (Abrate, 1998) 6

Figure 3.2 Indentation (Abrate, 1998) 8

Figure 3.3 Delamination and Fiber Orientations (Abrate, 1998) (Erbil, 2008) 10

Figure 3.4 Bending Cracks (a) and Shear Cracks (b) (Abrate, 1998) 11

Figure 3.5 The crack propagates from the upper layer to the lower layer (a) The crack propagates from the lower layer to the upper layer. (b) (Abrate, 1998) .. 11

Figure 3.6 Charpy and Izod test device (Thomas and Sorensen, 2018) 13

Figure 3.7 Specimen Fixing Positions on Charpy and Izod (Cantwell and Morton, 1991) 13

Figure 3.8 Schematic of the Drop Weight test device (Erbil, 2008) 14

Figure 3.9 Open and Close Curves on Contact Force Dısplacements Graphs 16

Figure 3.10 Penetration Threshold and Perforation 17

Figure 3.11 Contact force – Time Graphs 19

Figure 3.12 Dısplacements – Time Graphs 20

Figure 3.13 Velocity – Time Graphs 21

Figure 3.14 Absorbed Energy – Time Graphs 22

Figure 3.15 Absorbed Energy – Impact Energy 23

Figure 4.1 Stack and Bag Schematic 28

Figure 4.2 Figure Stack and Bag Process 29

Figure 4.3 Marking the Specimen for Cutting Process 30

Figure 4.4 Cutting with Wet Cutting Saw 30

Figure 4.5 Instron Ceast 9350-Optioned Version 31

Figure 4.6 Figure Specimen Fıxed for Experiment..... 33

Figure 4.7 Impactor..... 33

Figure 4.8 Contact Force-Dısplacements Graphs on Trials..... 34

Figure 4.9 Absorbed Energy-Time Graphs on Trials..... 35

Figure 5.1 (a) Contact Force–Displacements Curves Type 1 and (b) Dısplacements Value Type 1..... 36

Figure 5.2 Impactor Rebound at 10J, 20J and 30J but perforate at 40J and 50J Energy Level to Type 1 37

Figure 5.3 (a) Contact Force–Displacements CurvesType 2 and (b) Dısplacements Value Type 2..... 38

Figure 5.4 Impactor Rebound at 10J, 20J and 30J but perforate at 40J and 50J Energy Level to Type 2 38

Figure 5.5 (a) Contact Force–Displacements Curves Type 3 and (b) Dısplacements Value Type 3..... 39

Figure 5.6 Impactor Rebound at 10J, 20J and 30J ,reach penetration threshold at 40J but perforate at 50J Energy Level to Type 3..... 40

Figure 5.7 (a) Contact Force–Displacements Curves Type 4 and (b) Dısplacements Value Type 4..... 41

Figure 5.8 Impactor Rebound at 10J, 20J and 30J ,reach penetration threshold at 40J but perforate at 50J Energy Level to Type 4..... 41

Figure 5.9 Contact Force–Displacements Curves for all Energy Levels..... 42

Figure 5.10 Dısplacements–Time Curves for all Types..... 43

Figure 5.11 Contact Force–Time Curves for all Energy Levels..... 44

Figure 5.12 (a) Absorbed Energy-Time Curves Type 1 – (b) Absorbed Energy Values Type 1 44

Figure 5.13 (a) Absorbed Energy-Time Curves Type 2 and (b) Absorbed Energy Values Type 2 46

Figure 5.14 (a) Absorbed Energy-Time Curves Type 3 and (b) Absorbed Energy Values Type 3 46

Figure 5.15 (a) Absorbed Energy-Time Curves Type 4 and (b) Absorbed Energy Values Type 4 47

Figure 5.16 Absorbed Energy Curves for all Energy Levels 48

Figure 5.17 Absorbed Energy Values for all Energy Levels 49

Figure 5.18 (a) Energy Profile Methods for Type 1 and (b) Energy Profile Methods for Type 2 49

Figure 5.19 (a) Energy Profile Methods for Type 3 and (b) Energy Profile Methods for Type 4 50

Figure 5.20 Energy Profile Methods for all Types 50

Figure 5.21 Velocity-Time Curves for all Types 51

LIST OF TABLES

Page

Table 4.1 Resin and Hardener Properties 25

Table 4.2 Fiberglass Properties 25

,Table 4.3 Specimens orientation 26

Table 4.4 Consumables List 27

Table 4 5 Specimen Properties 31

CHAPTER ONE
INTRODUCTION

1.1 Introduction

The production of new materials, with the aim of combining two materials and using the best mechanical properties of these two materials in an optimum way, is at the center of material and engineering studies today.

Particularly in the last century, considering many damage criteria such as fatigue and creep, in addition to normal, shear, torsion, buckling and impact strength, in order to remain at the desired safety values in designs, in industry such as aviation and automotive, the excessive increase in the masses in the designs has led to the need for new materials.

For this purpose, combining two different materials to create new materials and making these materials lighter while providing the necessary strength has taken a great place not only in academia but also in industry.

For such reasons, composite materials have came in to our lives and studies on this subject have increased.

1.2 Purpose & Scope

Nowadays, it has become an important parameter how composite materials, which are frequently used in industry, aerospace and the automotive, will react to sudden single force under usage conditions, in addition to tensile compression and torsion. If the material is damaged by a single and sudden force on it, the entire design will need to be revised accordingly, so the study on the composie materials in this regard has been increased.

There are many studies on this subject in the literature. However, the reaction of woven composites against impact loading, which is the subject of this study, and its variation according to the fiber orientations in the structure of the composite, is still a subject that needs further study.

In this context, in this study, 4 types of composite samples were produced by E-glass and resin on different orientations then by applying impact energies of 10J, 20J, 30J, 40J and 50J to these samples, the effect of these orientation differences on the reaction during impact loading was tried to be explained.

CHAPTER TWO
PREVIOUS STUDIES

Since the woven E-glass reinforced resin composites to be used in this study are used in a wide range of areas in the industry, this has also been reflected in the universities. For this reason, in parallel with the needs in the industry, the reactions of these materials to impact tests have become the subject of study in universities.

In this scope; Atas and Sayman (2007) tested the samples they produced with 4 layers of woven E-glass fabrics and epoxy resin at impact levels between 4J and 45J and observed the entire process from the moment the first damage started to the final perforation and reported them. In these studies, penetration, perforation threshold and final perforations are clearly seen. They also showed in their study that the relationship between the impactor radius and the diameter and thickness of the sample or part to which the impact is applied is an effective parameter in determining the penetration or perforation threshold.

Mili and Necib (2001) produced samples with 10 layer of E-glass fabrics and Epoxy Resin with $[0_2/90_6/0_2]$, $[0_3/90_4/0_3]$ and $[0_4/90_2/0_4]$ orientation and tested it with 0.53 m/s, 1.47 m/s, 1.60 m/s ve 3.10 m/s impact velocity. In addition to these experiments, they also made theoretical calculations using the Hertz Contact Law. As a result of that studies, they reported that the difference between the theoretical calculation and the test results was due to the friction force on the rails that transmit the mass on the impact test device, and in addition, they determined that the increase in the fabrics in the [0] orientation increased the deformation values.

Avazpoor et al. (2023) produced 9-layers woven E-glass fabric in curves of 10 cm, 15 cm and 20 cm and tested it at 50J ,100J and 150J impact values. Then, they confirmed these tests with the Finite Element Model they modeled on ABAQUS. As a result of that study, they observed that as the radius of curvature of composites decreased, the contact force they applied to the impactor, the energy they absorbed and the loading and unloading time of the force coming from the impactor increased.

Sharma et al. (2019) to compare the impact behavior of composites in [90/-45/45/0] and [0/90/90/0] orientations, they produced with 4 layers of E-glass fabric and Epoxy Resin. They tested it at 5J, 10J, 15J, 20J, 25J and 30J energy levels. As a result of their studies, it was observed that the sample in the [90/-45/45/0] orientation, with increased orientation variation, give a higher contact force value, more resistant to initial damage, and shows higher rigid behaviour when the force-displacement curve was examined. Again, in the same orientation, the elastic deformation value is higher than the [0/90/90/0] orientation, while the permanent displacement value is smaller. Since the absorbed energy value is directly related to the amount of damage, the absorbed energy is higher in the [0/90/90/0] orientation, which has a larger delamination gap. In addition, when all contact times are examined, the contact time in the [90/-45/45/0] orientation is lower than the [0/90/90/0] orientation.

Belingardi and Vadori (2002) tested $[0/+60/-60]_s$, $[0/90]_s$ ve $[0/+45/-45]_s$ samples on their studies. As a result of the impact test performed by dropping a 20 kg impactor from a height of 25 mm, 50 mm, 100 mm, 150 mm, 175 mm, 200 mm, 225 mm, 250 mm and 300 mm, it was shown that the maximum contact force and first damage energy value obtained in the force displacement graph is not increase further after the impact threshold that would cause damage is exceeded.

Arıkan and Sayman (2015) produced E-glass fabrics in $[0/90]_{10s}$ orientation with thermoset and thermoplastic matrices and used Polypropylene and Epoxy Resin in their study to compare their impact behavior and tested them at 20J, 50J, 80J and 110J energy values. In that study where they applied repetitive loads at low energy values, they reported that thermoplastic matrix give higher life cycles under repetitive loads, even though the perforation thresholds is close.

Baucom and Zikry (2005) used E-glass fabric and Vinyl-Ester Resin in their study to compare the impact damage of 2D and 3D composites. The first one of the E-glass fabrics he used in this study is a 3D monolithic, orthogonal fabric, the second one is a 2-D woven fabric along the plane, and the third one is a [0/90] biax fabric. Increasing the strength in the axial direction of the composite caused the damage to increase in the radial direction and the deformation to decrease in the axial direction in the 3D

sample, compared to the other two types. Additionally, it was observed that the 3D sample had higher impact damage resistance and energy absorption ability.

Ataş and Liu (2008), in their study by revising the woving angles in woven composites, produced 20, 30, 45, 60, 75 and 90 degree fabrics instead of fabrics with a 90 degree difference between the weave and warp direction, and introduced a method for this manufacturing. Following the fabrication of this fabric, they produced composites in $[0/20]_4$ $[0/30]_4$ $[0/45]_4$ $[0/60]_4$ $[0/75]_4$ $[0/90]_4$ orientations with epoxy resin and subjected them to impact testing. As a result of these tests, they reported that the composites they manufactured at lower angles has less contact force value, more contact time, higher energy absorption and higher perforation threshold compared to those at higher angles.

Dogan and Arıkan (2017) applied impact tests at 25J, 50J, 75J, 100J and 125J values to the composites they produced by using thermoset and thermoplastic matrix to the sandwich structure they made from E-glass fabric and PVC Foam. It has been reported that thermosets make composites more rigid, but thermoplastics give better results in terms of deformation and load carrying ability.

Mathivanan and Jerald (2010) tested the samples produced from E-glass according to ASTM D3029 at impact velocity of 1.981 m/s, 2.426 m/s, 2.801 m/s, 3.132 m/s and 4.429 m/s. They determined the perforation limit and reported that crack initiation and delamination damage modes were observed.

CHAPTER THREE
METHODOLOGY AND ANALYSIS OF DATA

3.1 Contact Law

3.1.1 Hertz Contact Law

The moment when two isotropic solid parts contact each other elastically is modeled as a Hertzian impact problem. The normal pressure P occurring at this moment of contact is calculated by the following equation (Abrate, 1998)

$$P = P_0 \left[1 - \left(\frac{r}{a}\right)^2\right]^{1/2} \tag{3.1}$$

In this equation, P_0 is the maximum contact pressure value in the center of contact area, r is any point in the contact area, and a is the radius of curvature of the contact area.

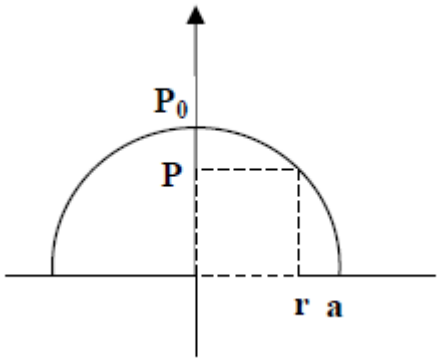


Figure 3.1 Pressure on Contact Area (Abrate, 1998)

In addition to the pressure value, the following formulations are used to calculate R and E values, which are other parameters needed when performing this modelling.

$$\frac{1}{R} = \frac{1}{R_1} + \frac{1}{R_2} \tag{3.2}$$

$$\frac{1}{E} = \frac{1 - {\nu_1}^2}{E_1} + \frac{1 - {\nu_2}^2}{E_2} \tag{3.3}$$

R_1 and R_2 are the radii of curvature of these two contacting parts. $E_1$and E_2 are the elasticity modules of these parts, and ν_1 and ν_2 are the poisson ratios of these parts.

After these formulations are obtained, the radius of curvature of the contact area a and the displacement α (indentation) are calculated. (Abrate, 1998)

$$a = \left(3\frac{PR}{4E}\right)^{1/3} \tag{3.4}$$

$$\alpha = \frac{a^2}{R} = \left(9\frac{P^2}{16RE^2}\right)^{1/3} \tag{3.5}$$

The maximum contact pressure is also calculated.

$$P_0 = \frac{3P}{2\pi a^2} = \left(\frac{6PE^2}{\pi^3 R^2}\right)^{1/3} \tag{3.6}$$

The law of contact force displacements can also be derived from these relations. This relation is considered as *Hertz Contact Law*.

$$P = k\alpha^{\frac{3}{2}} \tag{3.7}$$

Contact stiffness *k* is obtained as a result of the above equation.

$$k = \frac{4}{3}E\sqrt{R} \tag{3.8}$$

The contact time *t* is calculated according to the indentation α and instantaneous velocity *V* with the following equation. (Abrate, 1998)

$$t = \frac{2{,}943\alpha}{V} \tag{3.9}$$

3.1.2 Contact Law for Laminates

In impact tests performed on composites, the sample is not elastic and isotropic. During permanent indentation occurs at the moment of contact during these tests, there are differences in modeling the moment of contact, defined as loading, and the moment

of unloading, where contact is lost. This difference, after studies by Crook (1952), is defined by the following formulation

$$P = P_m \left[\frac{\alpha - \alpha_0}{\alpha_m - \alpha_0}\right]^{5/2} \tag{3.10}$$

In this formulation, P_m is the maximum pressure before the unloading section, α_m is the maximum deformation (indentation), α_0 is the permanent deformation (indentation)

If the critical deformation value symbolized as α_{cr} cannot be reached at any point during the loading, that is, if $\alpha_m > \alpha_{cr}$ cannot be achieved, the α_0 value is calculated as zero. Thus, no permanent damage occurs.

$$\alpha_0 = \alpha_m \left[1 - \sqrt[5]{\frac{\alpha_{cr}}{\alpha_m}}\right] \tag{3.11}$$

During performing an impact test, the absorbed energy value is a calculated value. This value is calculated with the following relation. In the theoretical infrastructure that creates this formulation, the total value of the area under the contact force-displacement graph is used.

$$U = \frac{2}{5} k\alpha^{2,5}{}_{max} \tag{3.12}$$

During elastic damage is observed in the composite plates up to a critical value at the time of contact, plastic damage is observed in the matrix when this threshold is exceeded. Once plastic damage begins to be observed, a new contact law comes into calculation.

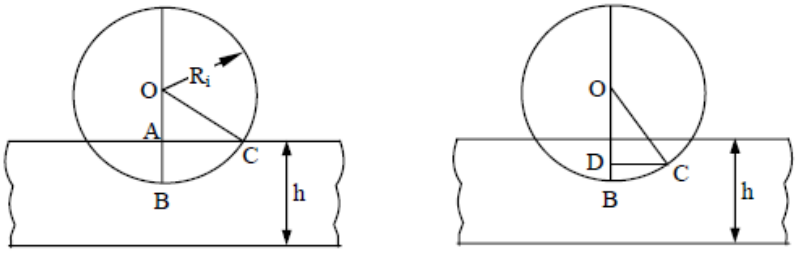


Figure 3.2 Indentation (Abrate, 1998)

$$\alpha = R_i - \sqrt{\left(R_{\mathrm{i}}^2 - R_C^2\right)} \tag{3.13}$$

In this new formulation, R_i is the impactor curvature radius, α is the indentation, and R_c is the contact radius.

$$R_c = \sqrt{2\alpha R_i - \alpha^2} \tag{3.14}$$

The contact radius is calculated as above. However, indentation is neglected because it is very small ($R_c \gg \alpha$) compared to the impactor radius.

$$R_c = \sqrt{2\alpha R_i} \tag{3.15}$$

The displacement caused by the impactor is calculated as follows.

$$\delta(r) = \alpha - R_i \left[1 - \sqrt{1 - \left(\frac{r}{R_i}\right)^2}\right] \tag{3.16}$$

In very small crushing values, the contact radius value is ignored because it is smaller than the impact tip radius of curvature

$$\delta(r) = \alpha - \frac{r^2}{2R_i} \tag{3.17}$$

In the direction perpendicular to the fiber orientation, the normal strain is distributed uniformly throughout the thickness of the composite material, the following assumption is made.

$$\varepsilon_{zz} = \frac{\delta(r)}{h} \tag{3.17}$$

If it is assumed that the material also elastic, the contact force is calculated as follows.

$$P = \frac{2\pi E}{h} \int_0^{R_c} \delta(r) r dr \tag{3.18}$$

E calculated here is the elasticity modulus perpendicular to the fiber. The elastic contact law is calculated with this value as follows.

$$P = \frac{2\pi R_i}{h}\alpha^2 \tag{3.19}$$

It is seen that the value calculated as contact force with this equation is greater than the which is calculated by Hertz Contact Law. (Abrate, 1998)

3.2 Failure Modes

After impact testing is applied to composite materials, basically three types of damage are observed. These damage modes are delaminations, matrix cracks and fiber fractures.

3.2.1 Delaminations

The damage mode called delamination is the separation of the matrix and the fibers forming the composite. Delaminations that are directly related to the orientations of the fibers are shown according to the orientations as shown in Figure 3.3.

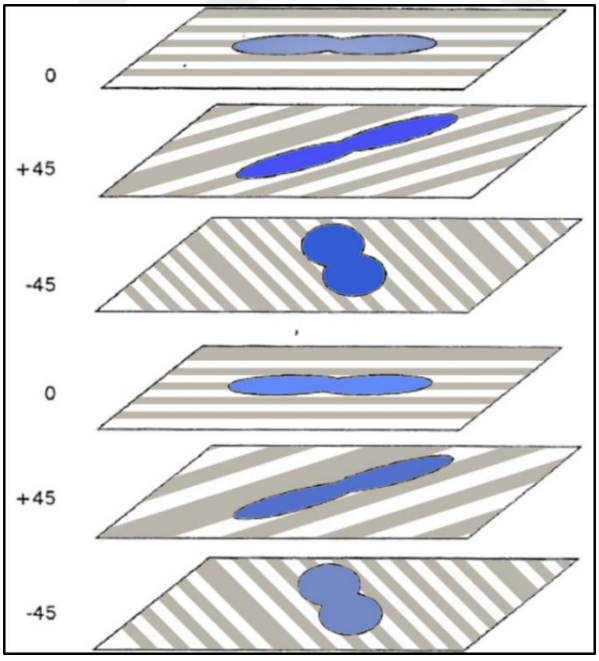


Figure 3.3 Delamination and Fiber Orientations (Abrate, 1998) (Erbil, 2008)

Delaminations are damages that occur only due to small discontinuities when a critical impact or load is exceeded, and this threshold is determined by experiments.

3.2.2 Matrix Cracks

After the load or contact on the composite, the resin cannot perform the appropriate toughness value and if its resistance to shear cracks is insufficient, matrix cracks begin in the structure and these subsequently cause delamination.

Matrix cracks occur in two types: bending cracks and shear cracks.

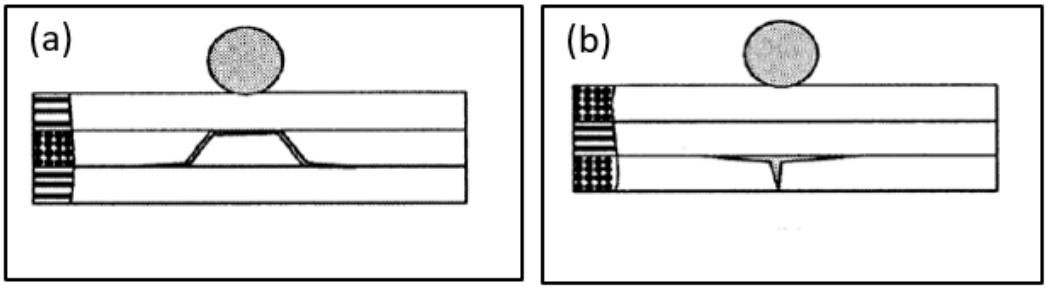


Figure 3.4 Bending Cracks (a) and Shear Cracks (b) (Abrate, 1998)

Considering the strength of the laminate perpendicular to the fiber as the critical threshold, bending cracks occur when the normal stresses in the plane exceed this critical threshold.

Shear cracks occur due to forces which is perpendicular to the fiber.

It is also observed in the top layer of thick samples. This damage occurs at the moment of first contact. The crack propagates from the upper layer to the lower layer. Even if the sample is very thin, bending forces occurring on the lowest surface cause matrix cracks. The crack propagates from the lower layer to the upper layer.

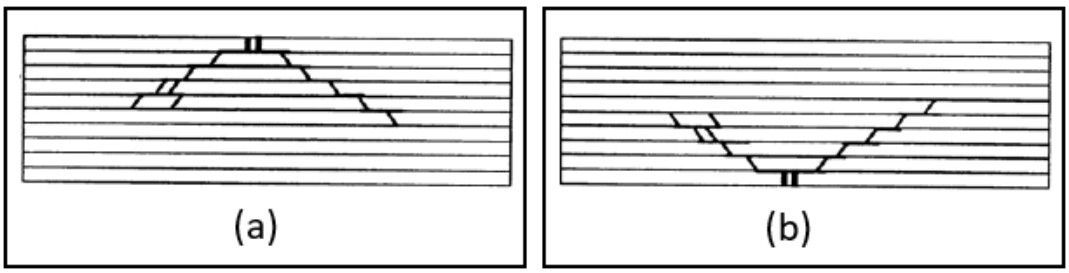


Figure 3.5 The crack propagates from the upper layer to the lower layer (a) The crack propagates from the lower layer to the upper layer. (b) (Abrate, 1998)

3.2.3 Fiber Fractures

Fiber cracks are generally not the first damage observed in composites. In fibers whose elastic modulus is generally higher than matrix materials, damage is generally observed after damage to the matrix.

In the impact test, at lower energy values the damage mode appears more like a matrix crack, while at higher energy values the damage mode is fiber breakage in addition to the matrix crack.

3.3 Impact Test Methods

Composite materials can be exposed to sudden and unexpected external forces because they are used in a wide variety of fields, from aviation to automotive, racing sports and wind turbines. For this reason, during the design process, it should be known whether the part to be produced can withstand these sudden forces.

For this reason, with the results obtained by applying impact tests on composite materials, potential changes in the structure of the part when exposed to any external force should be predicted at the design process. As a result of these predictions, these failure modes should be eliminated by choosing geometric changes, reinforcements (addition of additional fabric layer), different material preference or different orientation angle on the part.

3.3.1 Low Velocity Impact Test Methods

In the aviation industry, any equipment falling on the composite material during maintenance operations or production can cause many problems such as damage to the matrix and separation of fibers. In order to simulate these situations, impact tests are applied to composites at velocities between 1-10m/s. As a result of this applied impact test, errors that may occur on the composite can be predicted. (Gholizadeh, 2019)

3.3.1.1 Charpy and Izod Test

In the Charpy and Izod test, which are two very similar test methods, the Impactor is brought to the calculated height like a pendulum and hits the sample on which a

notch has been cut, transferring its energy to it. Figure 3.6 shows the schematic of the test device used in this test method.

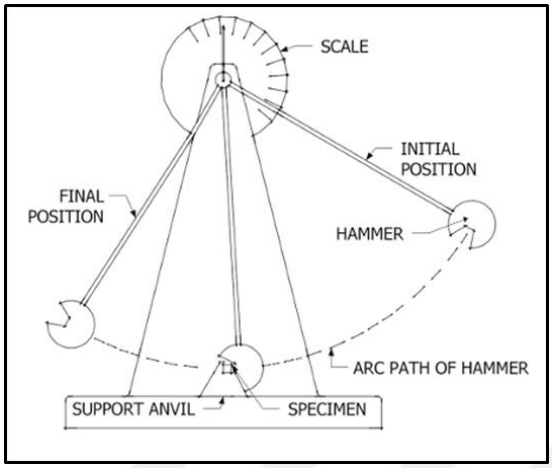


Figure 3.6 Charpy and Izod test device (Thomas and Sorensen, 2018)

The main difference between these two tests is the position of samples and the fixed place. There are many studies in the literature on this subject.

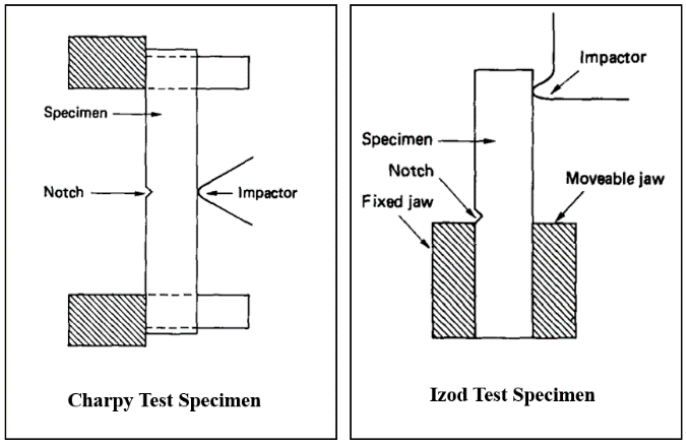


Figure 3.7 Specimen Fixing Positions on Charpy and Izod (Cantwell and Morton, 1991)

Shokrieh and Torabizadeh (2011) test E-glass specimens to Charpy Test with 10J, 20J and 30J with Charpy test device after hold the specimen -30^{o}C, -15^{o}C, 0^{o}C and 23^{o}C temperetures on 1 to 10 day. Among the samples kept at the specified temperatures for 10 days, the samples kept at lower temperatures absorbed less energy.

In addition, the damage modes that progressed as matrix cracks at room temperature take the form of fiber fractures and delamination at lower temperatures.

3.3.1.2 Drop Weight Tests

Another most commonly used impact test method is the impact test performed by dropping weight. In this test, the impactor is raised to a certain height and then dropped, hitting the sample and transferring the stored potential energy to the sample. Figure 3.8 shows the schematic of the test device used in this test method.

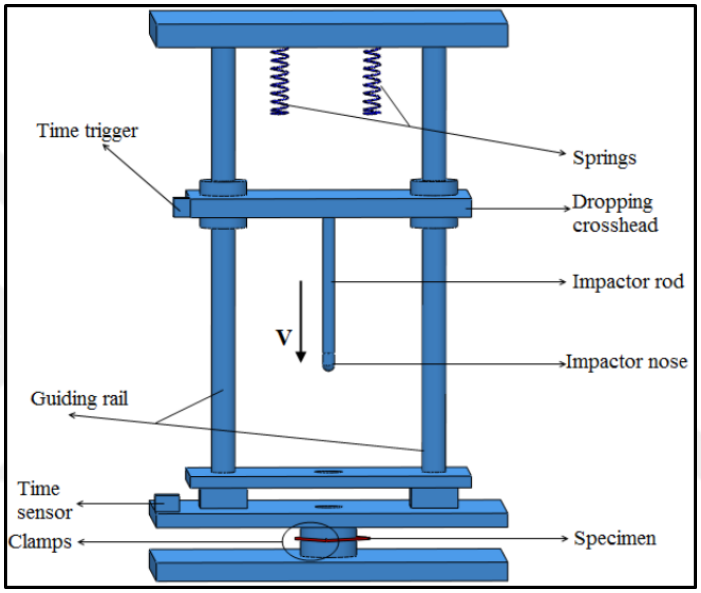


Figure 3.8 Schematic of the Drop Weight test device (Erbil, 2008)

In this study, tests were carried out with this method.

3.3.2 High Velocity Impact Test Methods

The reactions of the material in cases where a moving aircraft encounters hail, hits a flock of birds, or when parts bouncing off the ground hit composite surfaces at the time of landing are seen with high-velocity impact tests applied in the 10-100m/s velocity range. (Safri et al. 2014)

3.3.3 Ballistic Impact Test Methods

Ballistic impact tests, which are mostly applied to materials used extensively in military vehicles or aviation, range between 50-1000 m/s. (Razali et al. 2014).

Reddy Reddy et al. (2017) subjected the composites produced from E-glass and ultra-high molecular weight polyethylene (Dynema) fabric to low and high velocity impact tests. In this study, for the low-velocity impact test, impact velocities of 4.53m/s, 6.88m/s and 8.14m/s were used for energy values of 50J, 125J and 175J. For the high-velocity impact test, 355 m/s, 370 m/s and 385 m/s velocity values were used for 520J, 540J and 560J energy values and compared the strengths. It has been reported that the samples store more energy in these high-velocity tests, which are classified as ballistic due to the strain rate sensitivity in polymer composites.

3.4 Responses of Composites in Impact Tests

In this section, the reactions of composites subjected to low-velocity impact tests are explained in detail. Graphs used to interpret the results and damages occurring in composite samples according to the applied energies and information on how to make the interpretation are given.

3.4.1 Contact Force-Displacements Curves

Contact force-Displacements curves *(f-d)* are one of the most basic graphs used to determine impact reactions of composite samples.

As force is applied during the contact of the impactor and the sample, the f-d graph increases and reaches peak. While this peak is the maximum reaction force value shown by the sample, the increasing part of this graph is also called bending stiffness. If the fluctuations in the graph are observed very intensely during this increase, it generally indicates a matrix crack damage mode.

After the maximum load is reached, the graph begins to decrease. This is called the unloading section. The commonly observed damage mode at this section indicates damage to the fibers.

3.4.1.1 Open Curve-Close Curve

F-d curves are basically of two types. In these curves, called open curve and closed curve, closed curves can be interpreted as curves where the impactor hits and rebound the sample and open curves can be interpreted as curves where damage is observed.

In closed curves, the impactor hits the sample and most of the impact energy is absorbed by the sample, but the unabsorbed energy is spent during the rebound of the impactor.

In open curves, the impactor either penetrated or perforated the sample. In other words, displacements and damages are observed throughout the thickness.

In addition to these, transition points between open and closed curves are also visible. While some damage is present at these points, rebound is still present. So while some of the energy was absorbed both elastically and plastically, rebound was observed.

As the impact energy increases, the open curve continues to widen because deformation continues to increase. In samples where perforation occurs throughout the entire thickness, the end of the *f-d* graph shows an oscillatory horizontalization. This part is the energy spent on friction during the movement of the impactor within the sample. The reason for the oscillation is the reaction force in the irregular regime during friction. This part is removed from the graph and the area under the graph is calculated by drawing a representative parallel line from that point. The area under this graph gives the absorbed energy. It can also be said that after this part is reached, the sample cannot absorb more energy than this value. After this point, no matter how much the impact energy is increased, the maximum contact force and the amount of absorbed energy do not increase.

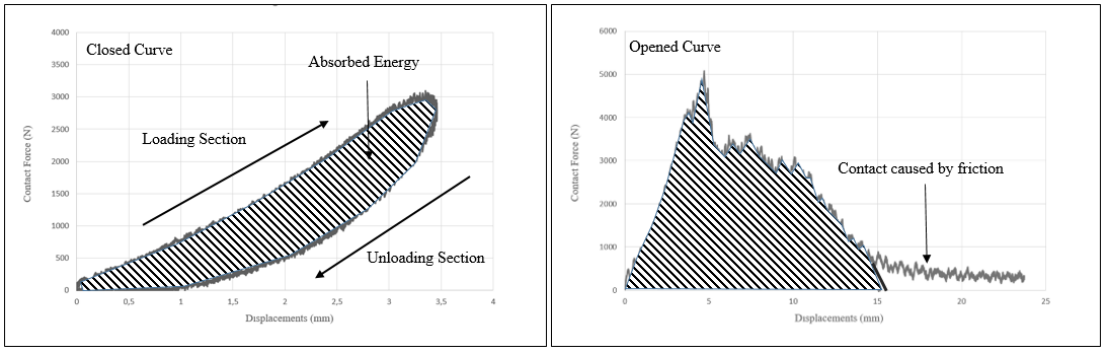


Figure 3.9 Open and Close Curves on Contact Force Displacements Graphs

3.4.1.2 Penetration and Perforation Thresholds

Basically, penetration is used to indicate the situation where the impactor penetrates and stuck the sample, and perforation is used to indicate the situation where the impactor pierces the sample.

The penetration threshold is the first energy value at which the impactor does not rebound from the sample, and the perforation threshold is the first energy value at which the impactor pierces the back surface of the sample.

Because of more layer of fabric used in aviation, turbine blade production or the automotive industry compared to the samples used in this experiment, at the penetration threshold, the sample is stuck in the impactor and buried inside. However, this is much more difficult to observe because the impactor diameter used in this study is much higher than the sample thicknesses.

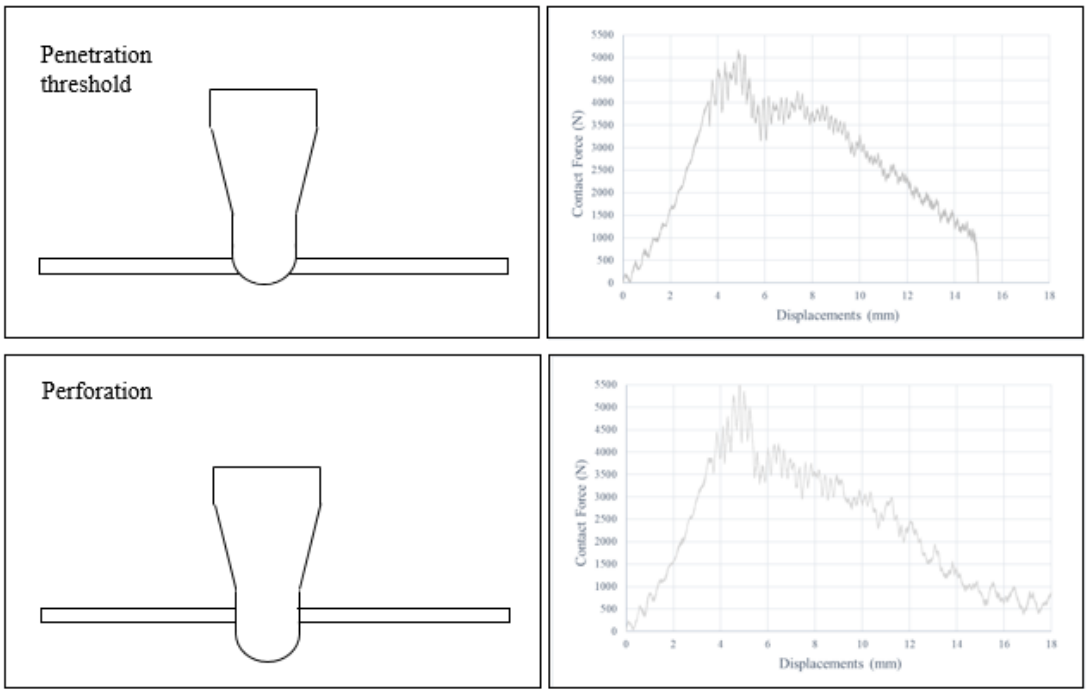


Figure 3.10 Penetration Threshold and Perforation

The penetration threshold is observed very close to the perforation threshold. Because when the first moment of the impactor does not rebound is examined, it was seen that the impactor reaches or comes very close to the back surface of the sample.

Although it is observed as a partial perforation here, it is important to know that this is accepted as the penetration limit. Because when the graphs are examined, a clear difference can be seen at the end of the *f-d* graph between the situation where perforation is clearly observed and the penetration threshold.

As the impactor pierces the sample at the perforation threshold, the reflection of the reaction force it encounters is seen at the end of the *f-d* graph. The sample continues to apply force to the impactor as the movement continues -completely penetrating- and this force can never be reach zero because the impactor never loses all its energy.

At the penetration threshold, the impactor stuck into the sample -especially in thin samples- reaches out from the back edge of the sample, but when it reaches it, it still stops before it can penetrate completely. Since the contact force becomes zero when the impactor loses all its energy, the force suddenly reaches zero at the end of the graph.

For this reason, acceptance was made as seen in the Figure 3.10.

3.4.2 Contact Force-Time Curves

When the Contact Force-Time curves *(f-t)* are examined, 3 different types of curves are obtained. When these curves are examined, the rebound curve can be reached where the force decreases to zero at the final value and there is not much oscilation during loading and unloading section. Because at the force values where these curves occur, not much damage occurs and the reaction force is more stable.

In the second type of curves, even if the force still reaches zero at the final value, penetration curves are obtained in which it can be interpreted that there is damage when the oscilations on the graph are examined. While it is basically interpreted that matrix damage occurs in the oscilations that occur during the force increase in the penetration curves, the damage that occurs on the fibers can be mentioned in the oscilations that occur at the unloading section.

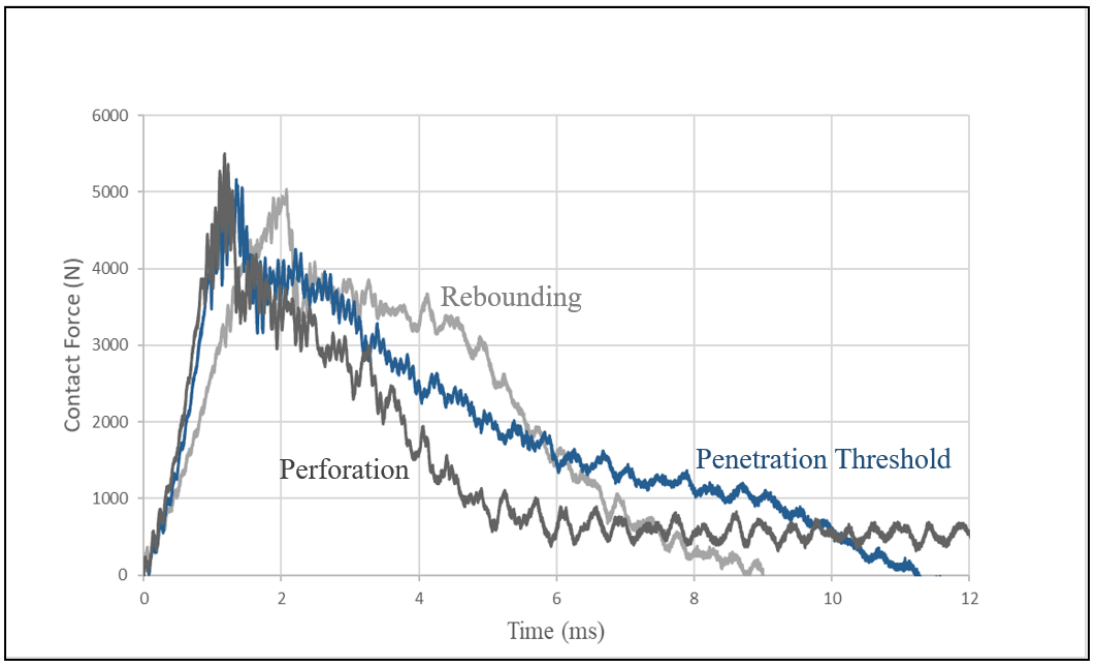


Figure 3.11 Contact force – Time Graphs

In the third type of curves, although oscilations are observed, the end of the force graph does not reach zero. This curve is the perforation curve and this horizontalization observed at the tip of the curve is the force caused by friction.

3.4.3 Displacements-Time Curves

When the displacement-time graphs *(d-t)* are examined, 3 different graphs are seen. These graphics are examined in three groups as rebound, perforation and penetration situations.

In the rebound curve, with time, the displacement first increases and then reaches zero again.

When the penetration graph is examined, the graph first increases with a larger slope over time, but this slope value decreases over time. In these samples where the impactor is stuck, this situation can be observed in the graph as the material displaced a certain amount and then absorbs all the energy of the impactor and remains motionless. Displacement increases with time, and the slope of this increase decreases continuously and eventually reaches zero.

In perforation curves, the displacement constantly increases and the curve itself and its slope never reach zero. The curve increases continuously.

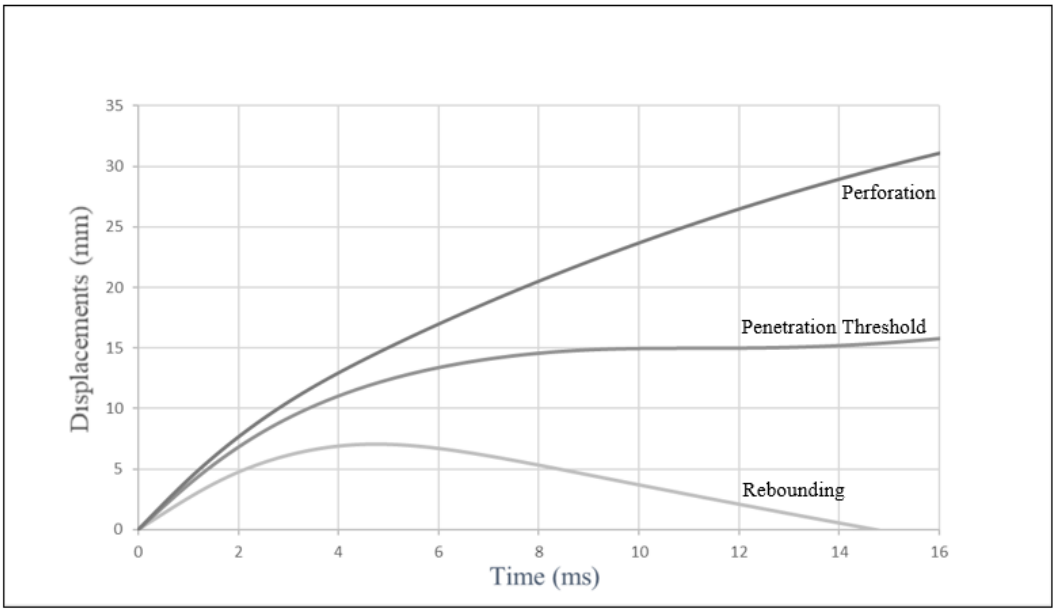


Figure 3.12 Dısplacements – Time Graphs

3.4.4 Velocity-Time Curves

When the velocity-time graphs *(V-t)* are examined, 3 different graphs are seen. These graphics are examined in three groups as rebound, perforation and penetration situations.

When the entire graph of the rebound curve is examined, the curve that starts at a lower velocity due to lower energy, impactor loses its velocity because it contacts the specimen and turns into a negative direction due to the rebound. It rebounded back at a slower velocity due to the absorption of some of the energy.

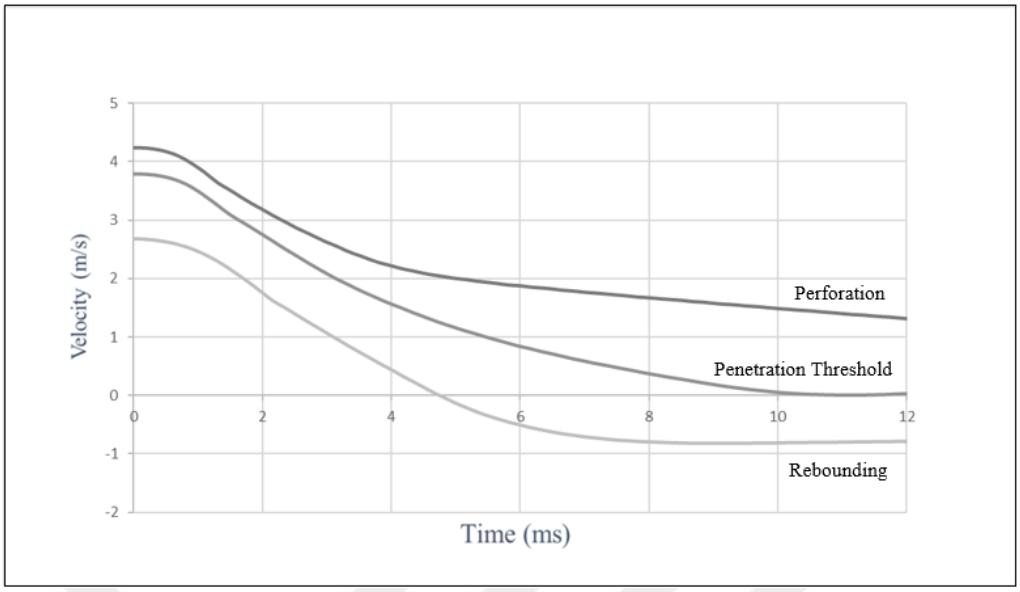


Figure 3.13 Velocity – Time Graphs

In the penetration graph, the decrease in velocity upon contact with the sample can be clearly read from the graph. As soon as the impactor gets stuck in the sample, the velocity is completely reach zero.

In the perforation graph, the impactor, which slows down at the moment of contact, continues its movement after piercing the sample and the velocity does not reach zero.

3.4.5 Absorbed Energy-Time Curves

When the absorbed energy-time graphs *(E_a-t)* are examined, 3 different graphs are seen. These graphics are examined in three groups as rebound, perforation and penetration situations.

The first graph obtained as a result of ıntegrating these areas is obtained for the rebound situation. In this curve, the E_a value first increases and then decreases. In case of penetration, the curve rises continuously and remains constant after penetrate specimen. For this reason, the curve becomes horizontal. In case of perforation, although the curve increases, the slope of this increase decreases after the moment of perforation. However, the E_a value on the graph is not become horizontal it continously increases.

For this reason, when perforation is observed, the E_a value is determined on the graph, and the point where the slope of the curve decreases is accepted as the E_a value. Because E_a observed from that point is the energy absorbed during friction.

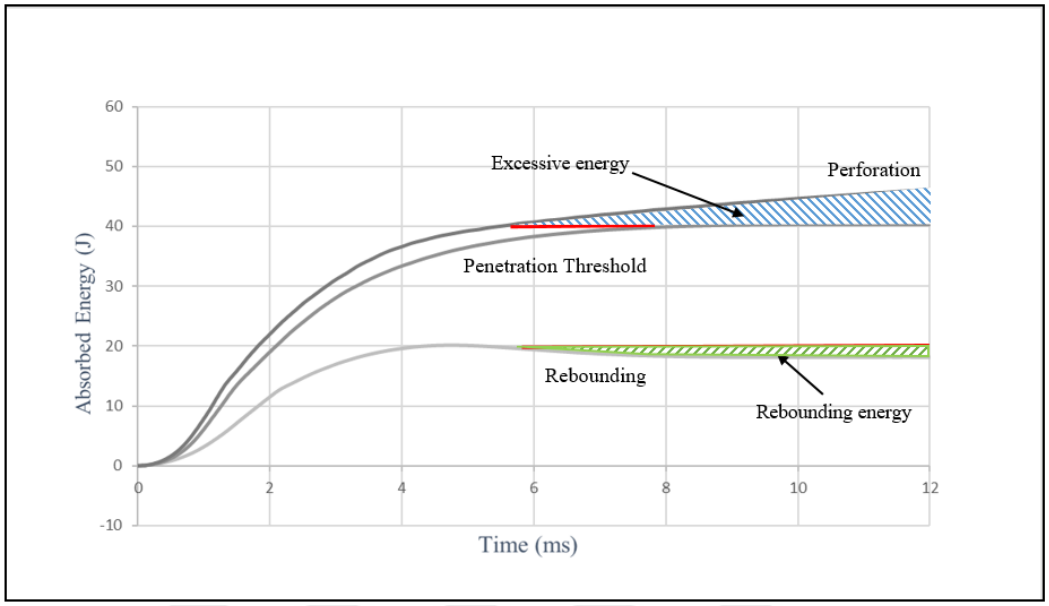


Figure 3.14 Absorbed Energy – Time Graphs

In the impact test method with weight drop, the impactor is raised to a certain height. Due to the impactor being removed and its mass, potential energy is stored on it.

$$E_i = mgh + mgd_{max} \tag{3.20}$$

In this relation, E_i is the impact energy, m is the mass of the impactor, h is the height of the impactor compared to the sample, and d_{max} is the maximum bending value on the sample as a result of the impactor hitting the sample.

Once the impactor is released, this potential energy turns into kinetic energy

$$mgh + mgd_{max} = \frac{1}{2}mV^2 \tag{3.21}$$

Since the displacement value is zero just before the contact between the impactor and the sample, the relationship becomes as follows when calculating the theoretical velocity at the moment of impact.

$$mgh = \frac{1}{2}mV^2 \tag{3.22}$$

If the velocity at the moment of impact is calculated from this relation,

$$V = 2\sqrt{gh} \tag{3.23}$$

3.4.5.1 Energy Profile Method

The energy profile method is a graphical method in which the relationship between E_a (Absorbed energy) and E_i (impact energy) is interpreted. This graph can be created and interpreted by seeing how much of the applied impact energy is absorbed.

In addition, by examining this graph, it can be interpreted at what energy values the impactor in contact with the sample rebounds, penetrated or perforated the sample.

The graph is shown in the Figure 3.15.

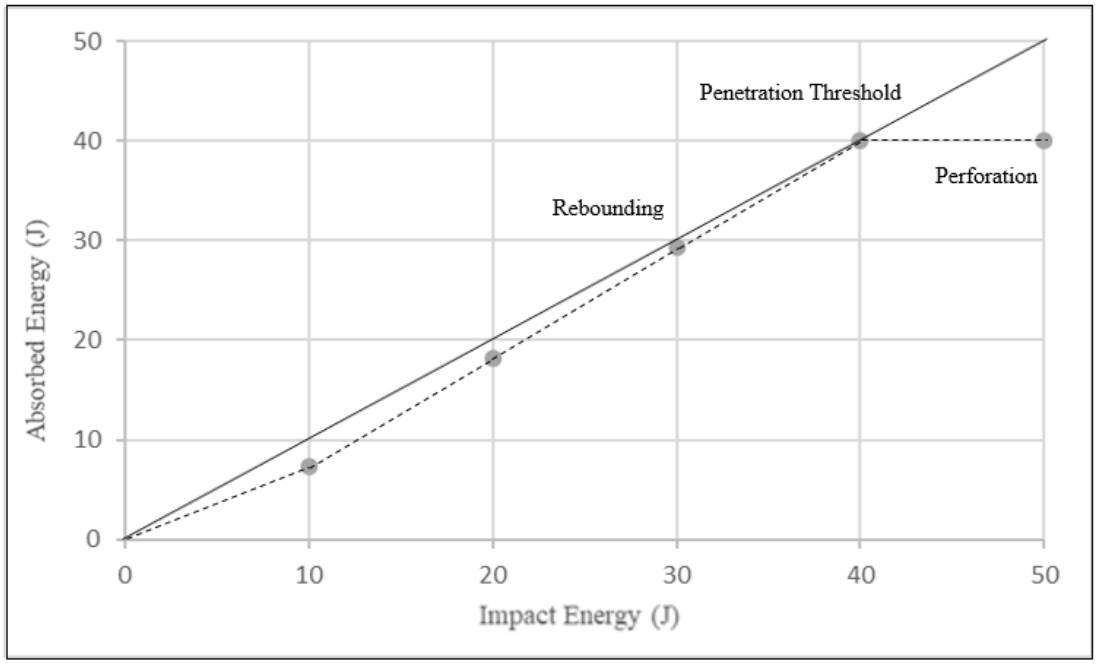


Figure 3.15 Absorbed Energy – Impact Energy

In this graph, the equal energy line obtained by connecting the points where E_a value and E_i values are equal is seen. The difference between Ea and Ei in the first

samples below this point is the excessive energy value and the energy spent for the rebound of the impactor.

It can be interpreted that as the E_a value approaches the equal energy line, the sample approaches the penetration threshold. It can be said that the penetration threshold has been reached when the E_a value is exactly on the equal energy line, that is, when all the applied energy is absorbed by the sample.

CHAPTER FOUR
PRE-EXPERIMENTAL PREPARATIONS

In this section, all processes from the composite production at Dokuz Eylül University Composite Manufacturing Laboratory to the impact test in Süleyman Demirel University – Innovative Technologies Application and Research Center are explained in detail. Also in addition to the E-glass fabrics, resins and hardeners used in sample production, the consumables and curing processes used are explained.

The main parts of the test device in which the impact test was performed are given, and in addition, the preliminary experiments carried out to determine the energy values to be applied to the samples are explained.

4.1 Sample Production

4.1.1 Fabric Preparation

Within the scope of this study, 300 g/m^2 woven E-glass fabric and Fibermak F-1564 Epoxy with Fibermak F-3486 hardener resin were used to produce composite samples in four different orientations for using in the tests.

Table 4.1 Resin and Hardener Properties

Material	Code	Viscosity (MPa.s)	Density (g/m^3)	Curing Time (at 80°C)	Mixture Proportion
Resin	F-1564	1200-1400	1,15	4 Hour	100
Hardener	F-3486	10-20	1	4 Hour	34

Table 4.2 Fiberglass Properties

Material	Warp Density Ends/cm	Weft Density Ends/cm	Mosisture Content **ISO 3344:2000**	Surface weight (density) [g/m^2] **ISO 3374:2000**	Loss on ignition[%] **ISO 1887:1995**	Breaking force [N] **ISO 3342:2000**
300g/m^2 Fiberglass	23	23	≤0.2%	± 10%	4,0÷5,5	<50

These produced composite types and orientations are given in the table below.

Table 4.3 Specimens orientation

Type	Orientation
Type 1	$[\ 0 / 90 / 0 / \overline{90}\ ]_s$
Type 2	$[\ 0 / 45 / 90 / \overline{45}\ ]_s$
Type 3	$[\ 0 / 30 / 60 / \overline{90}\ ]_s$
Type 4	[0 / 15 / 30 / 45 / 60 / 75 / 90]s

Optimization is an important parameter in composite production. This optimization focuses on reducing waste and losses as much as it focuses on production velocity. In mass or fabricated production, after determining the dimensions of the fabrics, nesting is applied to obtain the maximum amount of lamina in the desired size from a fabric roll. Siasos, A., & Vosniakos, G. C. (2014) also studied the effects of nesting applications on composite fabric cutting in their studies that include different approaches on this subject.

Because of fabric cutting is important, in this study, cutting plans were made at the certain angles for each sample in the 7-layer woven e-glass fabric cutting process in order to minimize material waste.

4.1.2 Consumables

The use of consumables amount in composite production is huge, and one of the most important issues in the work of engineers working in this industry is reducing the amount of consumables.

These consumables, which are inherent in the industry, also appeared during sample production. The table below gives the list of consumables used, starting from the bottom to the top layer.

Table 4.4 Consumables List

Consumable	**Purpose**
Teflon	Prevents the e-glass fabric from sticking to the mold/where it will be cured
E-glass	Woven Fabrics
Release Film	Provides easy separation of e-glass from consumables
Flow Mesh / Infusion Mesh	Provides resin flow and distribution
Bag	Separates the external environment from the area to be infused
Spiral Hose	Distributes the resin in the vacuum bagged area
Hose	Provides vacuum and on the other hand, it transmits the resin.
Vacuum Inlet	It is the part where vacuum and infusion reach the inside of the foil.

The first consumable material used in production is Teflon, which is laid to form an interface between the mold or the curing table and fibers, preventing adhesion.

Release film is a consumable material that allows the layers on the fibers to be peeled off easily. It has a porous surface.

Flow mesh / Infusion mesh is a fabric layer that allows the resin to flow linearly. It distributes the resin evenly with porous structure.

The bag, which is responsible for separating the vacuumed area from the external environment, prevents air from escaping after being vacuumed.

Spiral höse and höse are the only exit points in the vacuum area where the resin and air flow when vacuum is applied. They are connected to each other with a vacuum inlet.

4.1.3 Fabrication

Vacuum-Assisted Resin Infusion Molding (VARIM) method was used for sample production. The previously mentioned consumables and fabrics required for this production method were placed in the order given in the figure.

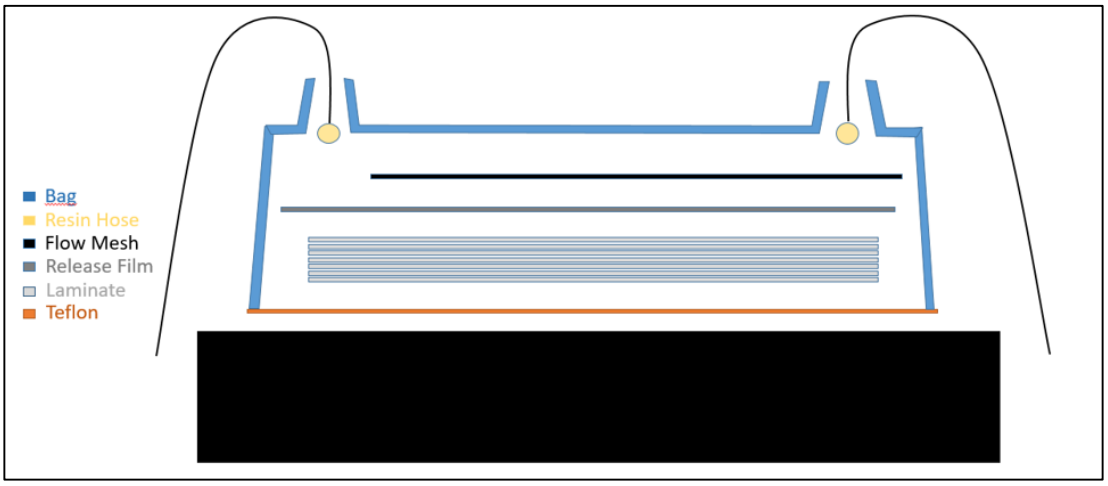


Figure 4.1 Stack and Bag Schematic

During sample production, Teflon material is laid on the bottom floor at the first stage. A notch is made at the bottom of the Teflon material. When the vacuum is turned on, the air under the Teflon is also sucked out. In this way, any gas that will remain there as a residue is prevented from deteriorating the composite geometry.

The laminate are then stacked precisely and the release fabric is placed on top of them. After the flow mesh placed to distribute the resin properly is placed on the top floor, the spiral hoses are placed at both ends.

After the fabric stack is completed, all fabrics are covered with bag. The bag is pierced at the points where the vacuum hose and infusion hose will be connected and the hoses are connected.

After the hoses are connected, paste is applied to these connection points. Since these are the places where the most leakage occurs during infusion and vacuum, the paste operations at these points are very critical. At this time, the vacuum is turned on and all the air in the foil is removed. Then the vacuum is turned off.

The mold is set to 45°C. In most applications, these temperature values are used on infusion process. Room temperature is not preferred. Because the resin reaches its optimum viscosity at this temperature value. In many industrial applications, when the resin cannot reach the desired places on the mold, one of the first places to check is the mold temperature. In addition to pastes that seal the foil are also more functional

at this temperature value. In this way, they are crushed more easily and show better adhesion and spreading.

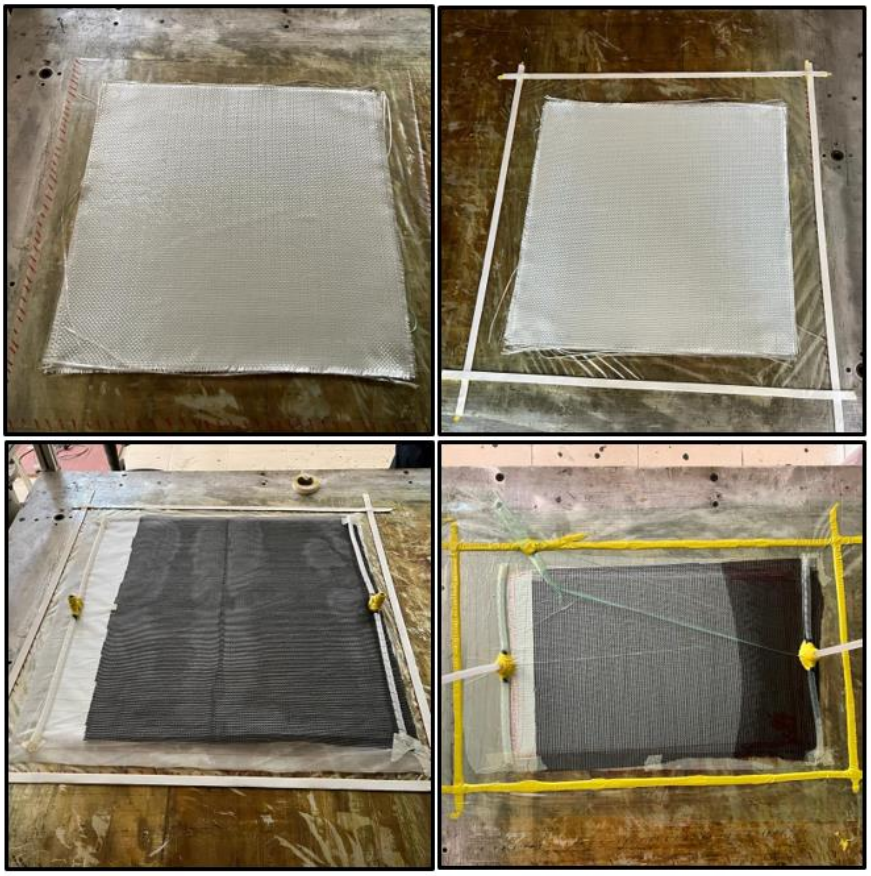


Figure 4.2 Figure Stack and Bag Process

After the waiting 10 minutes and if no change is observed in the barometer or no leakage sound is heard, the vacuum is turned off, it means that there is no leakage. Meanwhile, a 1/3 mixture of resin and hardener is prepared and infusion process started.



Figure 4.3 Marking the Specimen for Cutting Process

The curing table is cured at 80°C for 8 hours and composite production is completed. Then, 100x100mm^2 composite plates are cut with wet cutting saw and sample production is completed.



Figure 4.4 Cutting with Wet Cutting Saw

After all that production process , specimens properties given below.

Table 4 5 Specimen Properties

Specimen	Orientation	Thickness (mm) (± 0,04)	Weight (g) (±2)
Type 1	$[0/90/0/\bar{9}\bar{0}]_s$	1,11	30
Type 2	$[0/45/90/\bar{4}\bar{5}]_s$	1,12	31
Type 3	$[0/30/60/\bar{9}\bar{0}]_s$	1,12	30
Type 4	[0/15/30/45/60/75/90]	1,11	31

4.2 Test Device

The impact test device used in this study is Instron Ceast 9350. It can be shown in Figure 4.5.



Figure 4.5 Instron Ceast 9350-Optioned Version

On this machine, which is a more optioned version of the test device Instron Ceast 9350, the part marked 'A' allows impact between 757J and 1800J. Behind the motor-driven positioning system marked 'B' is the system marked 'C' that measures the entire mass that will hit the sample. According to the ISO 6603 standard, there is lubrication equipment marked with 'D' that eliminates friction effects during impact testing.

The impact energy to be applied can be determined by adding mass to the fixture labeled 'E'. In addition, since the impact energy can be increased by increasing the height rather than the mass, no additional mass was used in this study, and the result was achieved by making changes on the height of the impactor.

The tube marked 'F' allows the connection of different impactor. The anti-rebound system, which is used to prevent the impactor from hitting the sample and rebounding at low impact energies, and then falling back onto the sample, is marked 'G'. In this study, this system worked efficiently, especially at 10J, 20J and 30J values.

The feeding unit marked 'H' provides fast feeding of samples in studies involving a large number of samples, but was not used within the scope of this study. The mechanism used to quickly test 10 samples for a similar purpose is located in the area marked 'I'.

The heating and cooling system, which allows the testing of samples at different temperatures, is in the area marked 'J', and all these feeding cooling units and the closed volume where the contact occurs are created with the bottom sheet marked 'K'.

The produced samples were placed in the fixture in the testing device as seen in Figure 4.6.



Figure 4.6 Figure Specimen Fıxed for Experiment

Then, the impactor to be used in this study was installed on the testing machine. This impactor, also from the Inston brand, with a 10mm diameter tip in hemispherical geometry, was used throughout the entire study.



Figure 4.7 Impactor

The results obtained as a result of all this work are directly displayed at the very first stage with the help of a computer connected to the test device, and when a faulty test is performed, the user can directly notice it.

4.3 Detection of the Impact energy to be Applied

Within the scope of this study, more samples were produced from Type 1 orientation samples compared to other types of orientations. Because this production is done more here is to determine the penetration or perforation thresholds and predict the energy levels where differentiation will be observed by examining these damages and all their reactions to impact energy by performing a preliminary test at certain energy values on the Type 1 sample before the samples are tested.

For this reason, tests were applied to the Type 1 sample at energy values of 5J, 7.5J, 10J, 15J, 20J, 30J and 40J. As a result of these tests, it was aimed to predict energy levels that are likely to be perforation and penetration thresholds.

As a result of these trial tests, 5 different energy levels were determined to be applied to all samples.

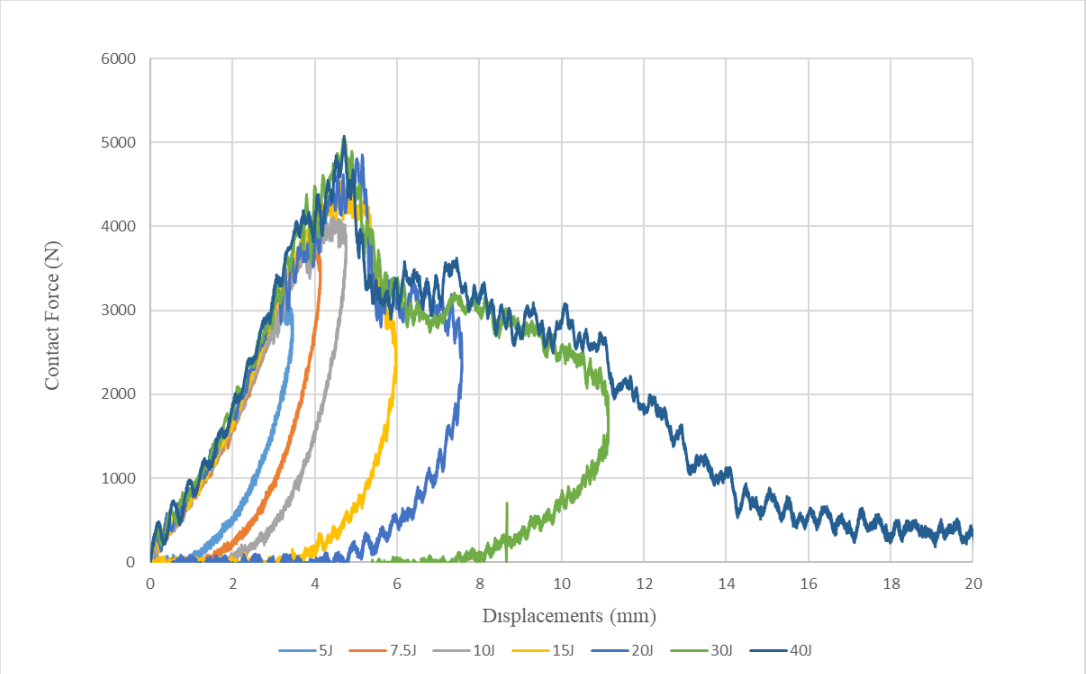


Figure 4.8 Contact Force-Displacements Graphs on Trials

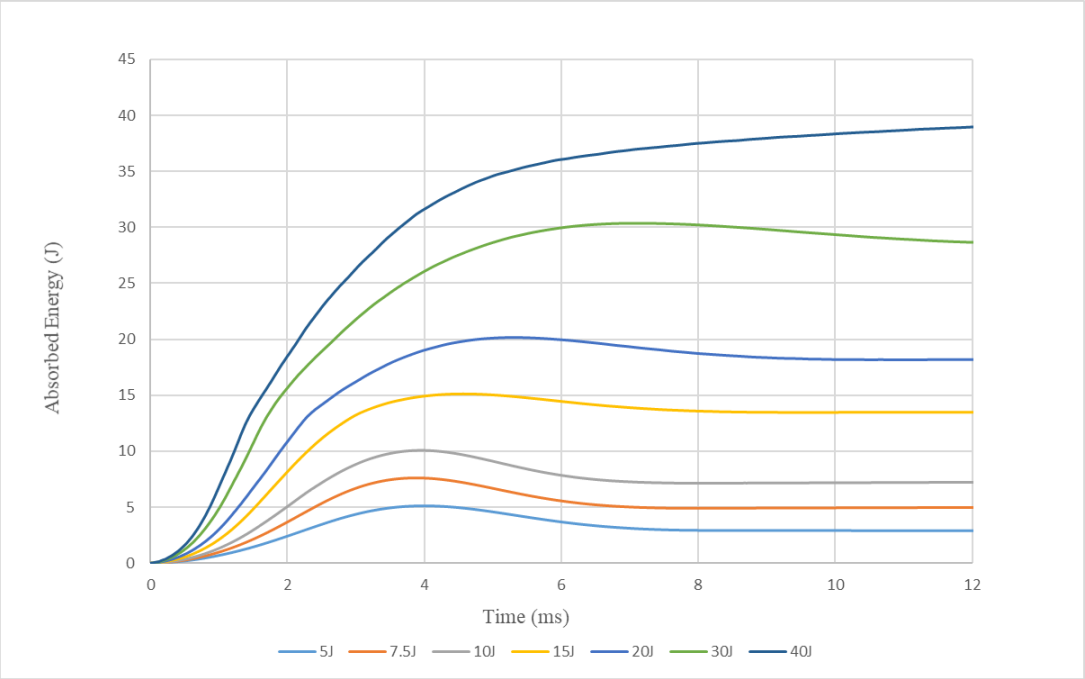


Figure 4.9 Absorbed Energy-Time Graphs on Trials

When the impact test is applied with a 40J impact, the contact force-displacements curve appears as an open curve for the first time. In addition, when the absorbed energy-time curve is examined, it is one of the first energy values where the distinction can be observed, as the graph shows a continuous increase and at one point, the energy absorbed due to friction constantly increases, similar to the perforation curves. For this reason, it was decided to use the exact value of 40J in the experiments.

Considering the possibility that no perforation would be observed at the 40J value in other orientation values, the 50J value was also added to the tests.

In the tests performed with 5J, 7.5J and 10J, no obvious differences or damages were observed. Since contact forces and displacements parallel to the energy increase were observed in all graphs at these low energy levels, 10J was chosen among these energy values.

After determining the 10J, 40J and 50J values, the 20J and 30J values were also determined to be applied in this study, as it was aimed that the applied energy values would increase linearly.

CHAPTER FIVE
RESULTS

5.1 Results

In this section, the impact tests carried out after all the preparations explained in the previous sections will be examined and the results will be interpreted.

Samples coded as Type 1 ($[0/90/0/\overline{90}]_s$) , Type 2 ($[0/45/90/\overline{45}]_s$), Type 3 ($[0/30/60/\overline{90}]_s$) and Type 4 ([0/15/30/45/60/75/90]) were cut in 100x100 mm^2 dimensions and impact forces of 10J, 20J, 30J, 40J and 50J were applied to these samples.

As a result, the reactions of the samples are displayed with into contact force-time, contact force-displacement, absorbed energy-time, etc. curves and these results were analyzed.

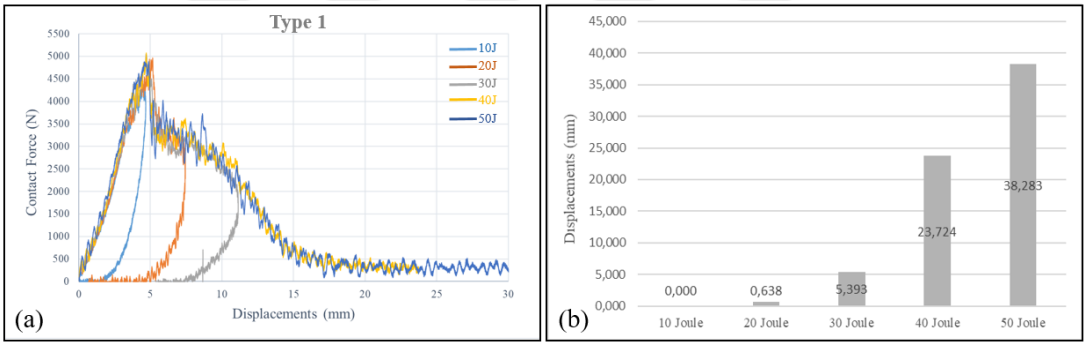


Figure 5.1 (a) Contact Force–Displacements Curves Type 1 and (b) Dısplacements Value Type 1

The contact force-displacements curve applied to the Type 1 sample is seen in the Figure 5.1. As mentioned before, one of the most basic parameters used when interpreting these curves is whether the curve is open or closed.

In these curves, at the first 10J, 20J and 30J values, the curve is a closed curve and no perforation is observed, and the impactor rebounds when it hits the sample. However, as the impact energy increased, permanent deformations began to be observed starting from the value of 20J.

However, starting from the energy value of 40J, the curve turned into an open curve, and as mentioned before, this means that when the impactor hits the sample, it no longer rebounds and perforates completely. Also, the increase in deformation is also noteworthy and increases dramatically with the increase in impact energy.

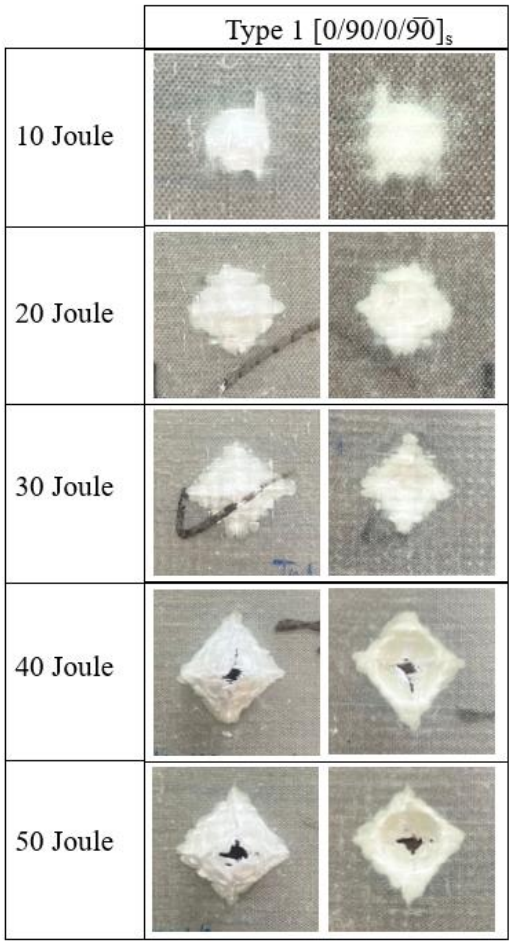


Figure 5.2 Impactor Rebound at 10J, 20J and 30J but perforate at 40J and 50J Energy Level to Type 1

When the curves are examined, the oscillation of the contact force value after it becomes horizontal at 40J and 50J is due to the unstable friction force applied to the edge of the impactor on that puncture surface while the impactor pierces the sample.

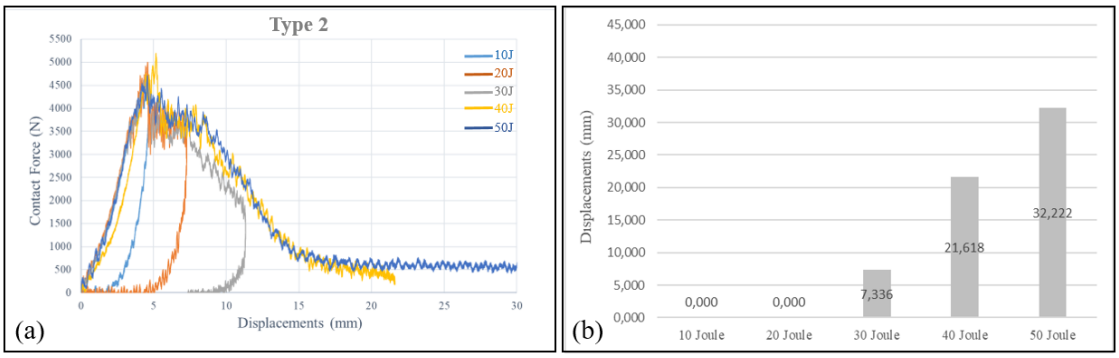


Figure 5.3 (a) Contact Force–Displacements CurvesType 2 and (b) Dısplacements Value Type 2

In the Type 2 sample, the impactor rebounded at values of 10J, 20J and 30J. However, no deformation was observed on the surface where the impactor applied the impact on the sample at 20J value. Type 2 performed more stable behavior than type 1 at this energy level.



Figure 5.4 Impactor Rebound at 10J, 20J and 30J but perforate at 40J and 50J Energy Level to Type 2

When the curve is examined at 40J and 50J values, it is seen that the sample is completely perforated. However, at the value of 40J, the curve close to zero during perforation, which is evidence that it shows more strength compared to Type 1.

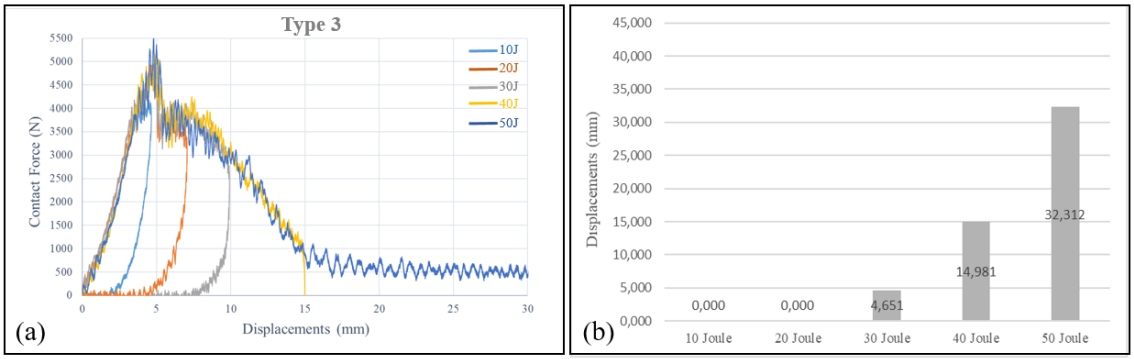


Figure 5.5 (a) Contact Force–Displacements Curves Type 3 and (b) Dısplacements Value Type 3

The Type 3 sample also rebounded the impactor at values of 10J, 20J and 30J, as expected. However, when the deformation data were examined, it was seen that the sample was less damaged in this first 30J value than the Type 2 and Type 1 samples.

The 40J was the energy value at which the graph in the Type 3 sample differed most dramatically compared to the Type 1 and Type 2 graphs. At this energy level, the contact force value did not become horizontal and suddenly reached zero. Because the impactor hit the sample, then penetrated a certain amount of the sample, but then stopped. Since the impactor lost all impact energy and did not completely penetrate the sample when it stopped, the sample apply reaction force until the impactor stopped, but after a while the reaction force stopped because the impactor was stuck. Since this energy value is where the impactor first penetrates, it is considered the penetration threshold.

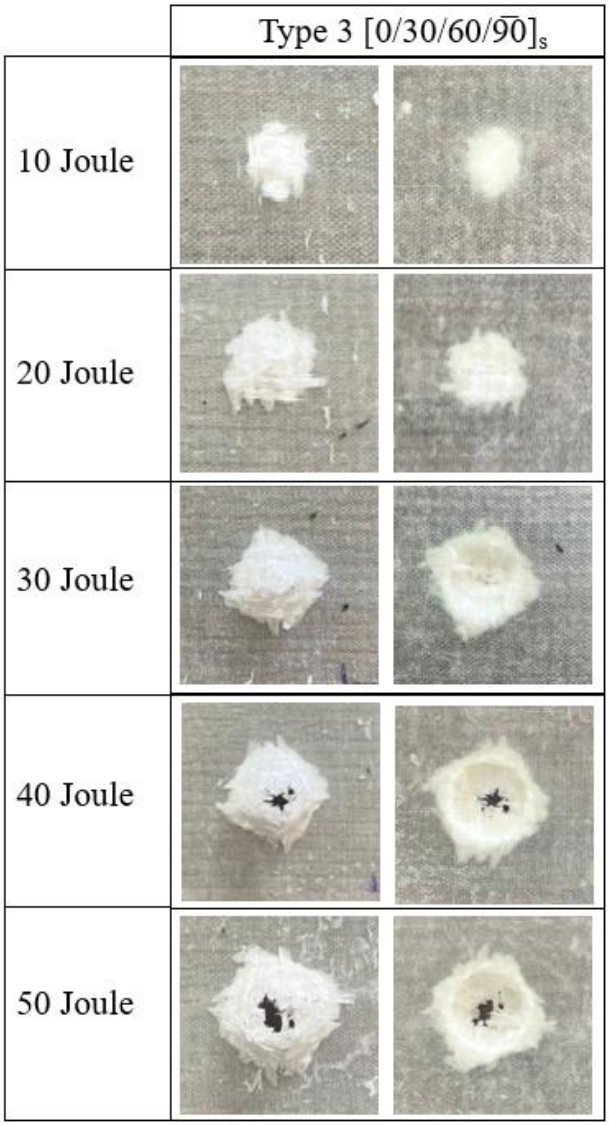


Figure 5.6 Impactor Rebound at 10J, 20J and 30J ,reach penetration threshold at 40J but perforate at 50J Energy Level to Type 3

However, as mentioned before, it is difficult to observe the difference between penetration and perforation thresholds in these tests, because the impactor diameter used in this test is very large compared to the sample thickness. Because after this energy value, perforation is observed because the sample is very thin - compared to the impactor. For this reason, it can also be referred to as the perforation threshold. However, in this study it was accepted as the penetration threshold.

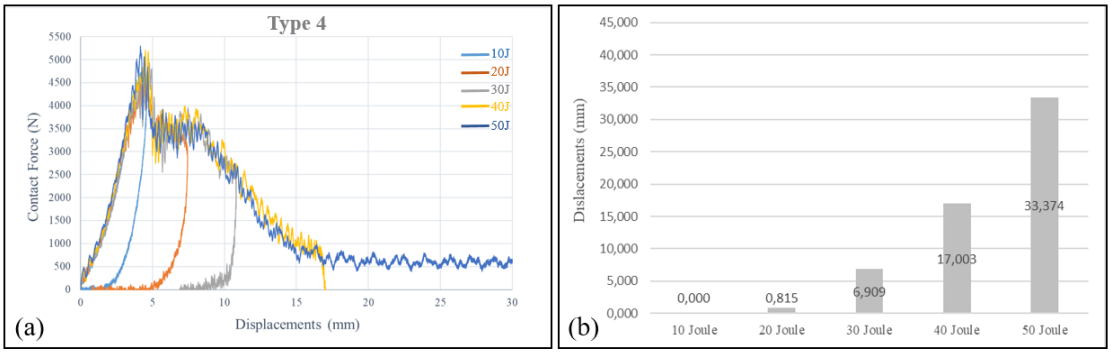


Figure 5.7 (a) Contact Force–Displacements Curves Type 4 and (b) Dısplacements Value Type 4

When the Type 4 sample was examined, rebound values of 10J, 20J and 30J were observed. At an energy value of 40J, it showed a behavior similar to Type 3 and reached the penetration threshold. At the value of 50J, perforation was observed, as in all samples.

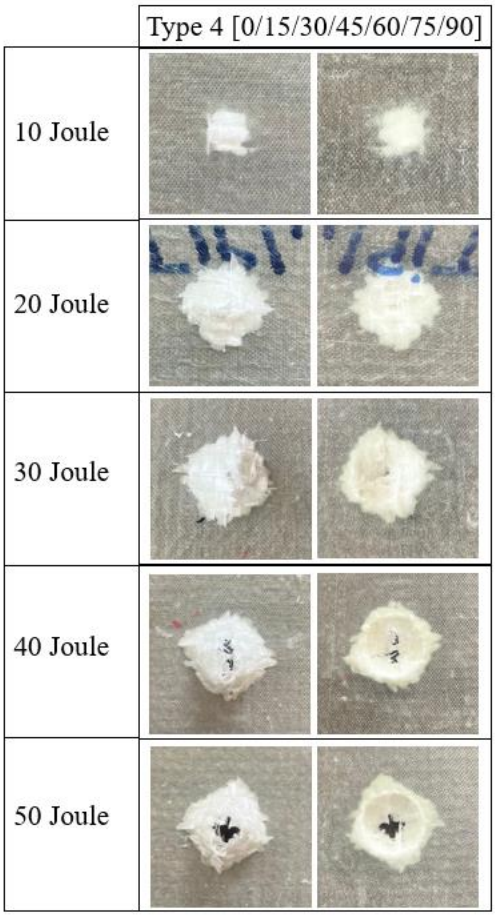


Figure 5.8 Impactor Rebound at 10J, 20J and 30J ,reach penetration threshold at 40J but perforate at 50J Energy Level to Type 4

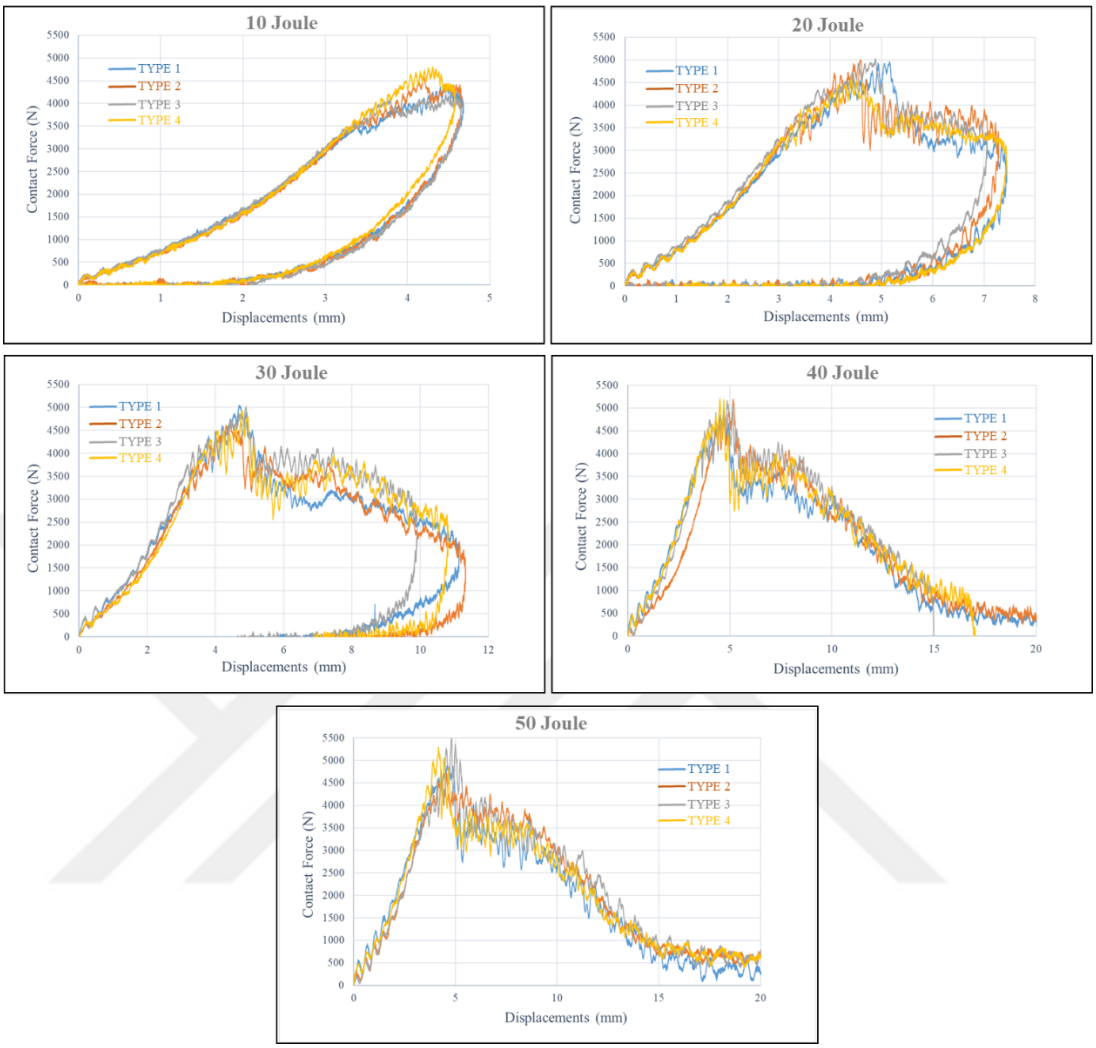


Figure 5.9 Contact Force–Displacements Curves for all Energy Levels

Figure 5.9. shows the contact force-displacement results of the samples for all energy values. When these results are examined with the previously mentioned results, the difference in the 40J value can be seen more clearly.

Type 4 and Type 3 on the penetration threshold on the 40J so the contact force reach zero suddenly end of the curves, but in same energy level Type 1 and Type 2 never reach zero because these specimens perforated.

However, the closed curves seen at the first 10J, 20J and 30J values and the open curve at 50J show that the samples give similar results in terms of damage at these values.

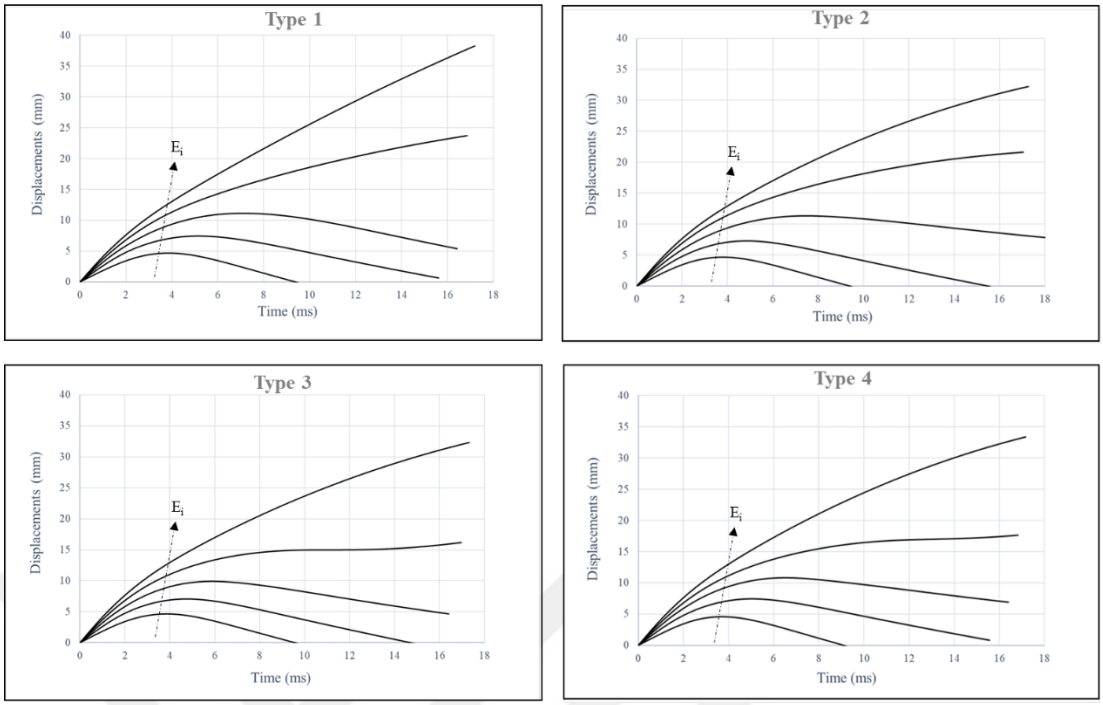


Figure 5.10 Dısplacements–Time Curves for all Types

The figure shows the changes in displacements compared to the energy values applied to the samples. The rebounds in the 10J, 20J and 30J can also be seen on these curves in all samples.

The displacements reach zero on 10J energy levels for all types. But as the impact energy increase, the displacements get raise.

The continuous increase on the displacements of the graph at 40J and 50J is the result of perforation in Type 1 and Type 2 samples. In these curves, deformation values never reach zero.

In Type 3 and Type 4 samples, the value of 40J, where the displacement does not increase at all after a value, is evidence of the penetration threshold. Again, the perforation at 50J in these samples can also be seen on these graphs.

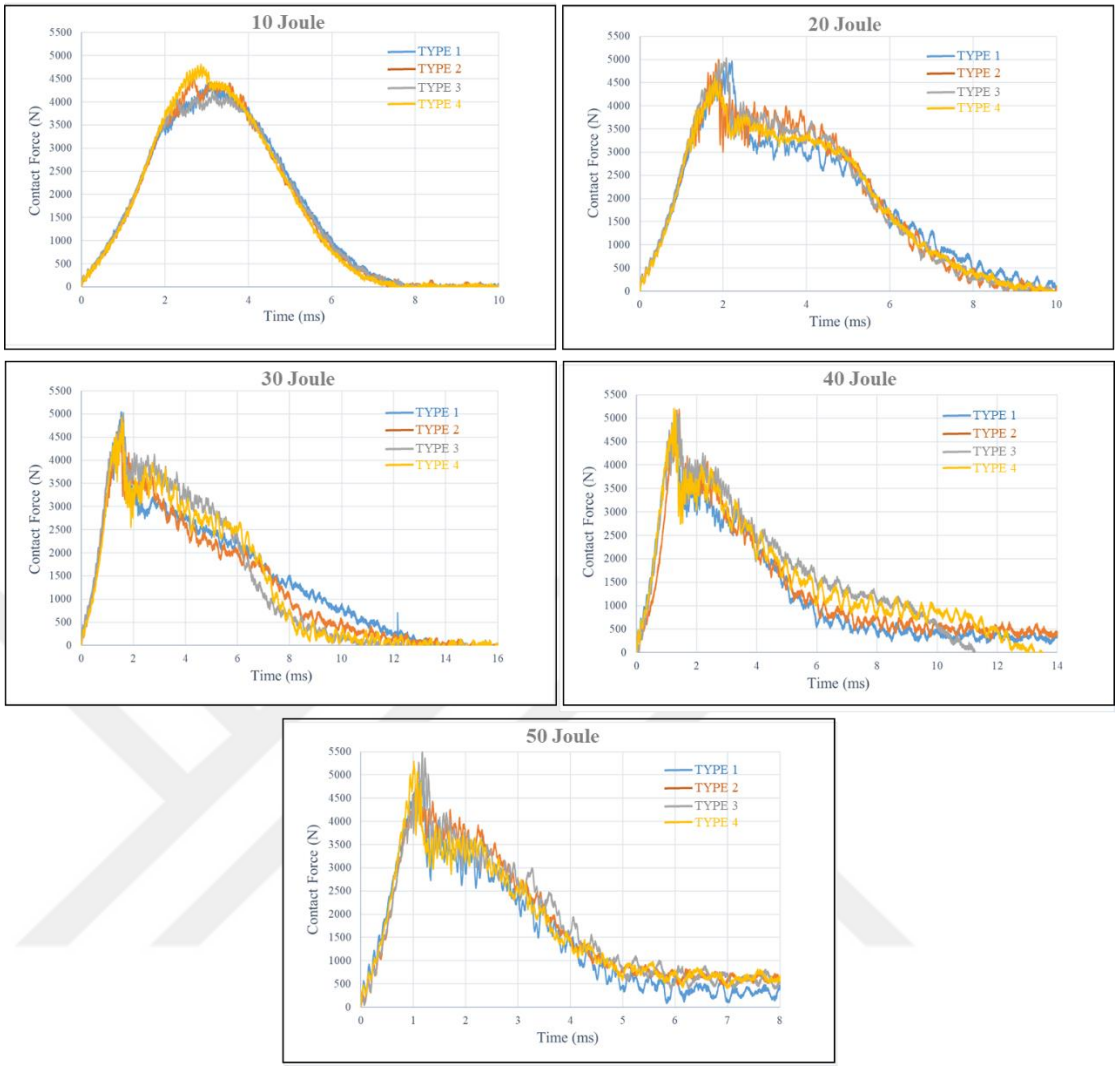


Figure 5.11 Contact Force–Time Curves for all Energy Levels

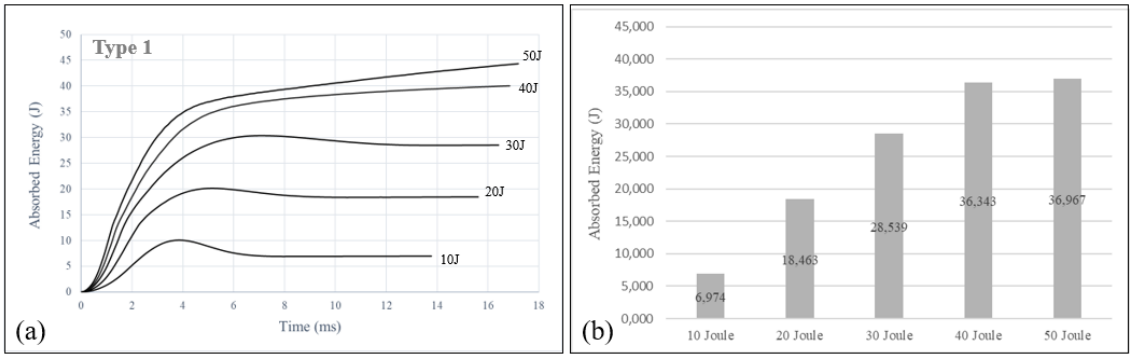


Figure 5.12 (a) Absorbed Energy-Time Curves Type 1 – (b) Absorbed Energy Values Type 1

When the absorbed energy - time graphs are examined, as mentioned before, in the samples where the impactor rebounds, all the impact energy applied is transmitted to the sample in the first stage, and a part of it is spent on elastic deformation. As this energy is released due to this non-permanent elastic deformation, the impactor is pushed back and rebound is observed.

In these curves, which is another evidence that rebound is observed at 10J, 20J and 30J values in the Type 1 sample, the sample completely absorbs the energy value coming on it in the first stage and then pushes the impactor back. For this reason, some of the applied energy is spent on the rebound of the impactor.

When the samples are examined, the proportional decrease in the energy spent on rebound up to 30J compared to the applied impact energy shows that the deformation on the sample is not elastic but also plastic, in other words, the deformations are permanent.

At 40J and 50J values, the graph first shows an increase at a high slope value, and then after a while, the curve continues to increase with a lower slope angle. The moment when this slope angle decreases and the curve increases with a lower slope angle is the moment when the sample is perforated, and the energy absorbed after this point is due to the energy spent by friction while the impactor perforated the sample.

At the contact force-displacements curves, the unstable moments when the graph starts to become horizontal and oscillates, reflect like that on the absorbed energy graphs.

Because of the perforation was observed again at the 50J value applied on the sample, the same amount of energy was absorbed as the perforation result at 40J.

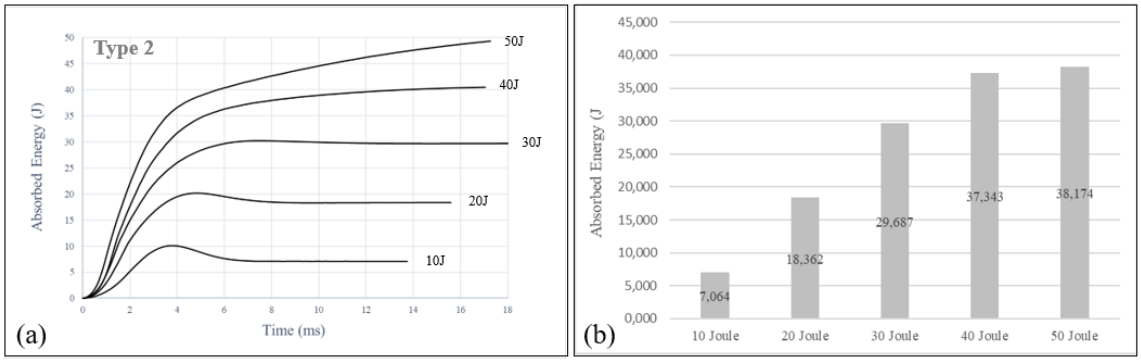


Figure 5.13 (a) Absorbed Energy-Time Curves Type 2 and (b) Absorbed Energy Values Type 2

Because of the Type 2 sample rebounded the impactor at 10J, 20J and 30J values, as expected, the curves were as shown in the figure. The fact that the curve observed at 40J and 50J values continues to increase after a point is an indication of perforation.

However, since the 40J value is the energy level where perforation is observed for both Type 1 and Type 2 samples, it can be used to compare these two samples.

As shown before, when the point where the second increase rate begins is determined on the curves, this point indicates the real absorption value. While this energy value is 36.343 in the Type 1 sample, it is read as 37.343 in the Type 2 sample. The Type 2 sample absorbed more energy, even if only slightly.

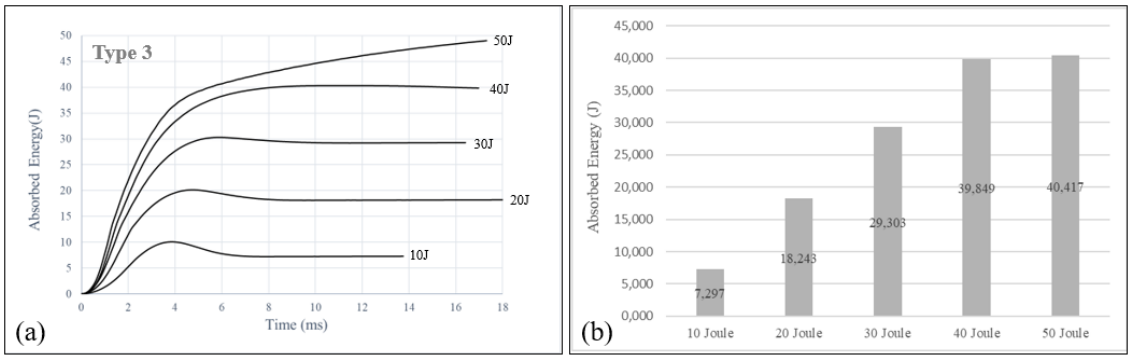


Figure 5.14 (a) Absorbed Energy-Time Curves Type 3 and (b) Absorbed Energy Values Type 3

Type Although the Type 3 when compared with other samples absorbed more energy, but similar to other samples, it rebounded the impactor at 10J, 20J and 30J. However, the energy level where the Type3 sample differs from other curves is 40J.

Since the curve was not perforated, it did not pass into the secondary increase curve and became completely horizontal. It was also the first energy value at which all applied energy value was completely absorbed. These results are not surprising since the penetration threshold assumption has been made before. It was predicted that the sample could not absorb more energy than this energy value, and when the 50J curve was examined, it was seen that it could not.

At all energy values to be applied more than the accepted threshold of 40J, the sample will absorb this energy value and will then be completely perforated.

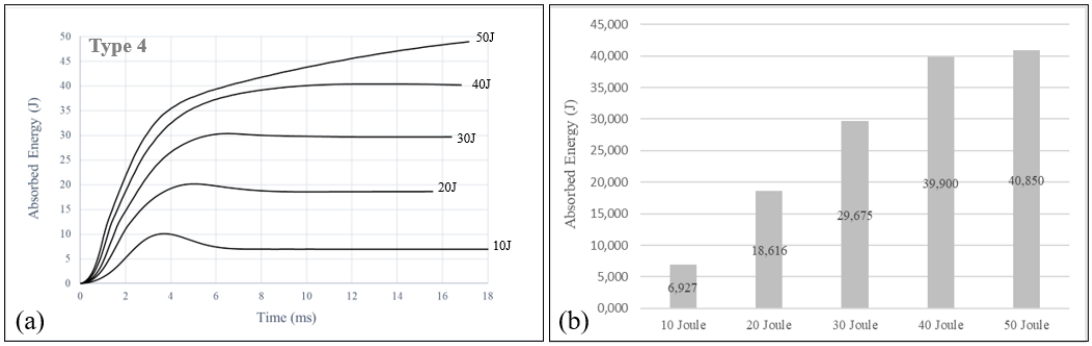


Figure 5.15 (a) Absorbed Energy-Time Curves Type 4 and (b) Absorbed Energy Values Type 4

As expected, Type 4 absorbed more energy than Type 1 and Type 2 and gave results close to Type 3.

The sample became horizontal at 40J and reached the penetration threshold. It will and has been perforated at every energy value applied on it. This perforation is observed when the 50J graph is examined, and again, as in Type3, the sample could not absorb more energy than the 40J value at which it reached the threshold.

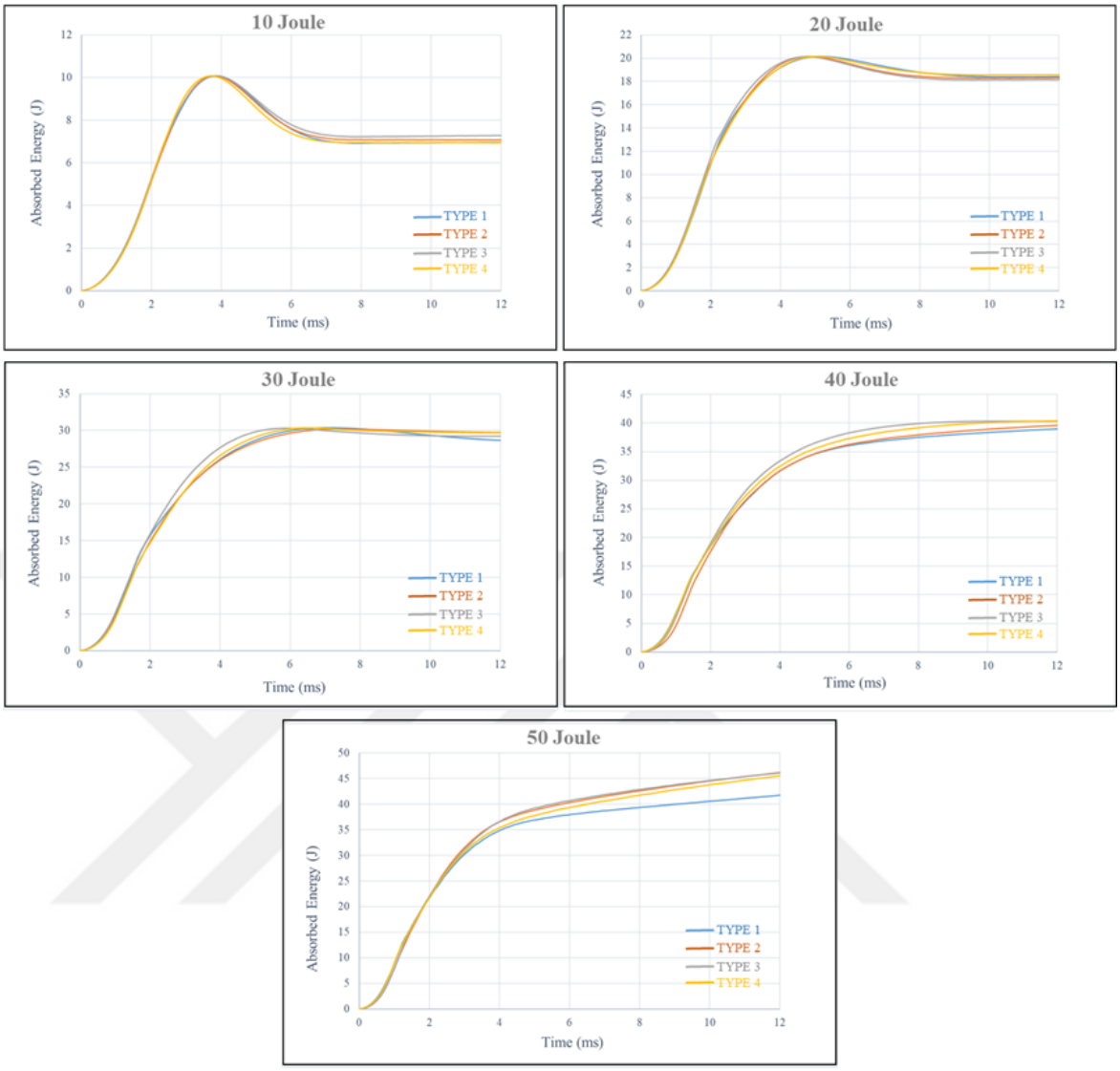


Figure 5.16 Absorbed Energy Curves for all Energy Levels

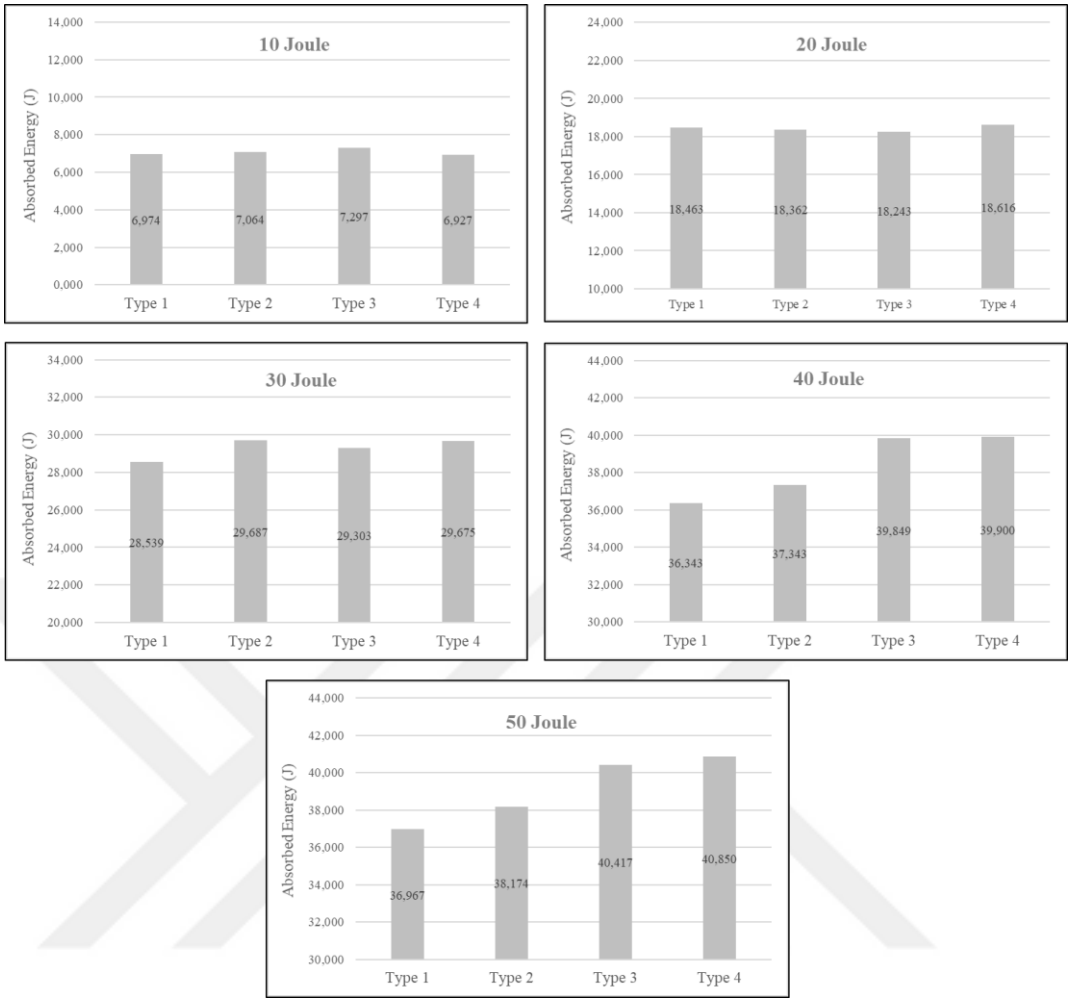


Figure 5.17 Absorbed Energy Values for all Energy Levels

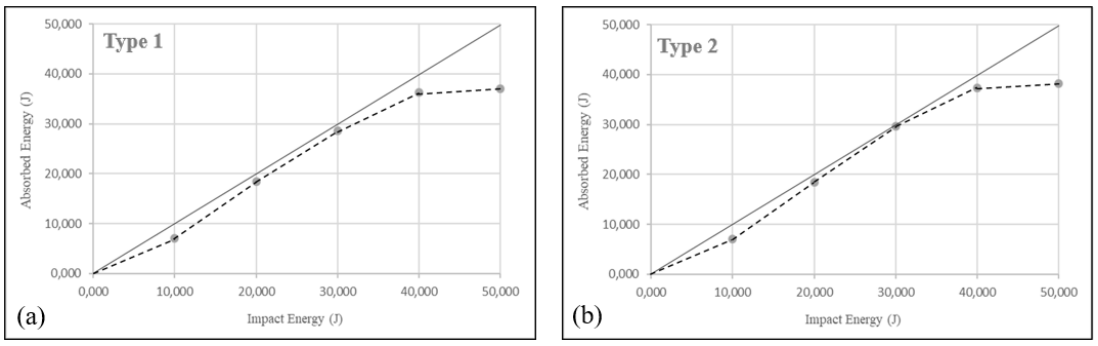


Figure 5.18 (a) Energy Profile Methods for Type 1 and (b) Energy Profile Methods for Type 2

When a linear line is drawn between absorbed energy and impact energy, energy absorption differences between types are seen. As the applied energy increases, the reaction of the samples also differs.

It was previously stated that the Type 1 and Type 2 samples could not absorb all the energy because the sample impactor rebounded at values of 10J, 20J and 30J in the first three tests. However, it can be seen in these curves that the rate of absorbed energy gradually increases at these energy values, which is a result of the decrease in the elastic deformation rate mentioned before.

The sample started to deviate from this linear line at the value of 40J, which is because, as is known, perforation was observed. At 50J, it has completely moved away.

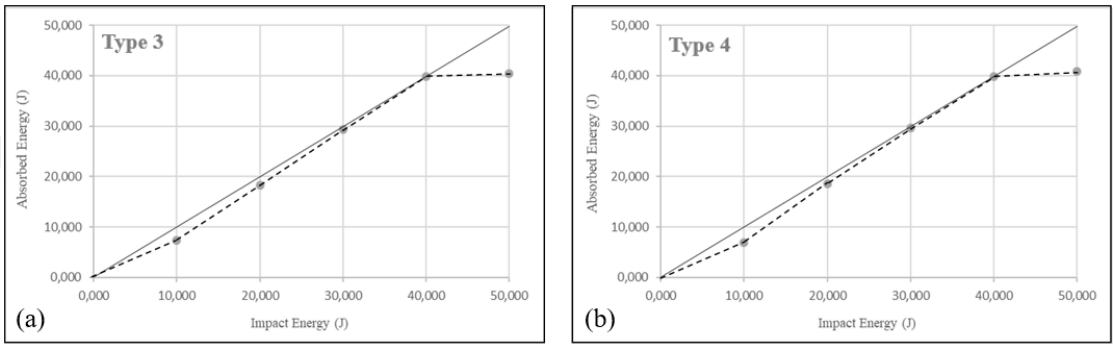


Figure 5.19 (a) Energy Profile Methods for Type 3 and (b) Energy Profile Methods for Type 4

In Type 3 and Type 4 samples, the energy absorbed curve value converges to the linear line up to 40J and is the same at 40J. Since this is the penetration threshold, the result is not a surprise.

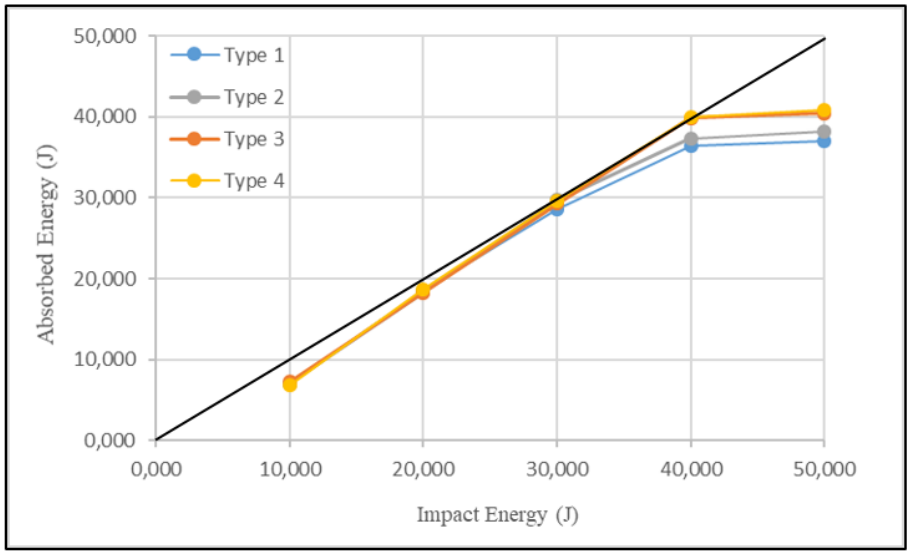


Figure 5.20 Energy Profile Methods for all Types

The amount of decrease in the energy spent on rebound compared to the 40J value indicates that the perforation threshold is approached. It is also expected that the sample penetrated at 40J cannot absorb more energy, therefore the curve became horizontal at 50J and showed that it cannot absorb more energy than 40J.

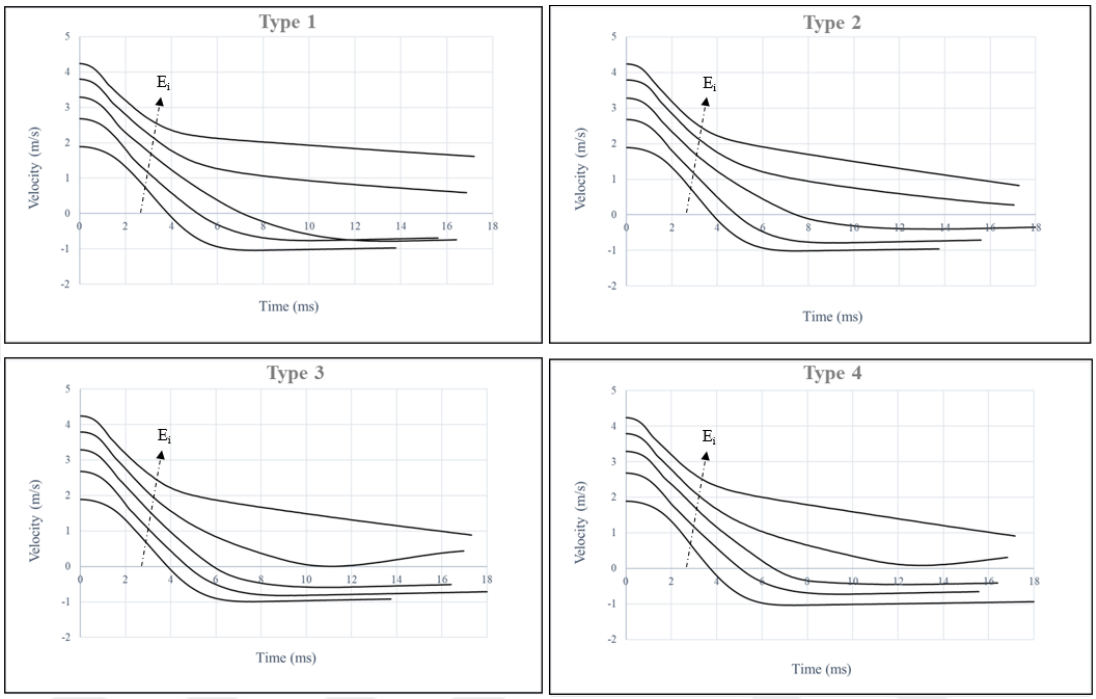


Figure 5.21 Velocity-Time Curves for all Types

When the velocity time graphs are examined, all samples velocities curves pass into the negative region due to rebound on 10J, 20J and 30J

While the perforation effects can be seen in this graph at 40J and 50J values, where the velocity is never reach in Type 1 and Type2, the graph reaching zero in Type 3 and Type 4 samples at 40J is another evidence of the penetration threshold. Although, perforation was observed in these samples at 50J value, which can be seen from the graph.

5.2 Conclusions

As a result of these tests, all findings were collected and the following conclusions were reached.

The Type 1 sample produced with the $[0/90/0/\overline{90}]_s$ orientation rebounded the impactor at energy levels of 10J, 20J and 30J. At values of 40J and 50J, it was completely perforated. The first permanent deformation on the sample started at 20J value.

The Type 2 sample in the $[0/45/90/\overline{45}]_s$ orientation rebounded the impactor at the energy levels of 10J, 20J, 30J and was perforated at the 40J and 50J. Permanent deformation started at 30J impact. Even though it showed permanent deformation values close to Type 1, it was not damaged at 20J, and when the force-displacement graph was examined, Type 2 performed more resistance than perforation at 40J.

The Type 3 sample produced in the $[0/30/60/\overline{90}]$s orientation rebounds at 10J, 20J and 30J. However, at 40J the sample reaches the penetration threshold. If the value is 50J, the sample is perforated.

Type 4, produced in the [0/15/30/45/60/75/90] orientation, also rebounds the impactor at 10J, 20J and 30J. At a value of 40J, it reaches the perforation threshold. At a value of 50J, it is completely perforated.

Type 3 and Type 4 samples absorbed more energy at the critical 40J energy level compared to Type 1 and Type 2 samples. Because the penetration threshold is higher in Type 3 and Type 4.

Variation of layer orientation increases the energy absorbed on the sample up to a certain angle changes and reduces deformation, but that variation cannot increase the strength after a certain angle changes.

When the energy profile method is examined, the absorbed energy value approaches the linear line as it approaches the penetration threshold and is exactly above the line at the penetration threshold.

No matter how much impact the sample exposed to above the penetration limit, it cannot absorb more energy than that threshold. After that threshold, it undergoes perforation and this does not change no matter how much the energy increases.

REFERENCES

Abrate, S. (1998) Impact on composite structures. Cambridge University Press, United Kingdom, 289 s.

Arikan, V., & Sayman, O. (2015). Comparative study on repeated impact response of E-glass fiber reinforced polypropylene & epoxy matrix composites. *Composites Part B: Engineering*, *83*, 1-6.

Atas, C., & Liu, D. (2008). Impact response of woven composites with small weaving angles. *International journal of impact engineering*, *35*(2), 80-97.

Atas, C., & Sayman, O. (2008). An overall view on impact response of woven fabric composite plates. *Composite Structures*, *82*(3), 336-345.

Avazpoor, E., Kazemian, A. H., & Rahmani, H. (2023). Numerical and experimental investigations on the low velocity impact properties of glass fiber reinforced epoxy composites: effects of radius of curvature. *Fibers and Polymers*, *24*(9), 3289-3298.

Baucom, J. N., & Zikry, M. A. (2005). Low-velocity impact damage progression in woven E-glass composite systems. *Composites Part A: Applied Science and Manufacturing*, *36*(5), 658-664.

Belingardi, G., & Vadori, R. (2002). Low velocity impact tests of laminate glass-fiber-epoxy matrix composite material plates. *International Journal of Impact Engineering*, *27*(2), 213-229.

Cantwell, W. J., & Morton, J. (1991). The impact resistance of composite materials—a review. *composites*, *22*(5), 347-362.

Crook, A. W. (1952). A study of some impacts between metal bodies by a piezo-electric method. Proceedings of the Royal Society of London. Series A. Mathematical and Physical Sciences, 212(1110), 377-390.

Dogan, A., & Arikan, V. (2017). Low-velocity impact response of E-glass reinforced thermoset and thermoplastic based sandwich composites. *Composites Part B: Engineering*, *127*, 63-69.

Erbil, E. (2008). *Impact loading in laminated composites* (Doctoral dissertation, DEÜ Fen Bilimleri Enstitüsü).

Gholizadeh, S. (2019). A review of impact behaviour in composite materials. *International Journal of Mechanical and Production Engineering*, *7*(3), 2320-2092.

Mathivanan, N. R., & Jerald, J. (2010). Experimental investigation of woven E-glass epoxy composite laminates subjected to low-velocity impact at different energy levels. *Journal of Minerals & Materials Characterization & Engineering*, *9*(7), 643-652.

Mili, F., & Necib, B. (2001). Impact behavior of cross-ply laminated composite plates under low velocities. *Composite structures*, *51*(3), 237-244.

Razali, N., Sultan, M. T. H., Mustapha, F., Yidris, N., & Ishak, M. R. (2014). Impact damage on composite structures–a review. *Int. J. Eng. Sci*, *3*(7), 08-20.

Reddy, T. S., Reddy, P. R. S., & Madhu, V. (2017). Response of E-glass/epoxy and Dyneema® composite laminates subjected to low and high velocity impact. *Procedia engineering*, *173*, 278-285.

Safri, S. N. A., Sultan, M. T. H., Yidris, N., & Mustapha, F. (2014). Low velocity and high velocity impact test on composite materials–a review. *Int. j. eng. sci*, *3*(9), 50-60.

Sharma, A. P., Khan, S. H., & Velmurugan, R. (2019). Effect of through thickness separation of fiber orientation on low velocity impact response of thin composite laminates. *Heliyon*, *5*(10).

Shokrieh, M. M., Torabizadeh, M. A., & Fereidoon, A. (2011). Dynamic failure behavior of glass/epoxy composites under low temperature using Charpy impact test method.

Siasos, A., & Vosniakos, G. C. (2014). Optimal directional nesting of planar profiles on fabric bands for composites manufacturing. *CIRP Journal of Manufacturing Science and Technology*, *7*(3), 283-297.

Thomas, R. J., & Sorensen, A. D. (2018). Charpy impact test methods for cementitious composites: Review and commentary. Journal of Testing and Evaluation, 46(6), 2422.